Technetium retention by gamma alumina nanoparticles and the effect of sorbed Fe^{2+}

Natalia Mayordomo[a,*], Diana M. Rodríguez[a], Dieter Schild[b], Konrad Molodtsov[a], Erik V. Johnstone[c], René Hübner[d], Salim Shams Aldin Azzam[a], Vinzenz Brendler[a], Katharina Müller[a,*]

[a] *Helmholtz-Zentrum Dresden - Rossendorf (HZDR), Institute of Resource Ecology, Bautzner Landstrasse 400, 01328, Dresden, Germany*
[b] *Karlsruhe Institute of Technology (KIT), Institute for Nuclear Waste Disposal (INE), Hermann-von-Helmholtz-Platz 1, 76344, Eggenstein-Leopoldshafen, Germany*
[c] *Innovative Fuel Solutions (IFS), 89031, North Las Vegas, NV, USA*
[d] *Helmholtz-Zentrum Dresden - Rossendorf (HZDR), Institute of Ion Beam Physics and Materials Research, Bautzner Landstrasse 400, 01328, Dresden, Germany*

GRAPHICAL ABSTRACT

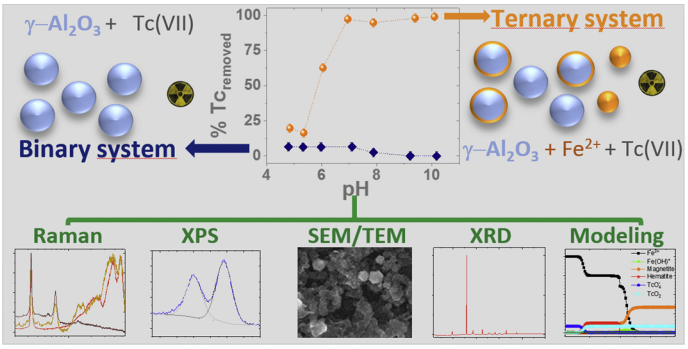

ARTICLE INFO

Editor: Deyi Hou

Keywords:
Technetium
Al_2O_3
Reduction
Sorption
Immobilization

ABSTRACT

Technetium (Tc) retention on gamma alumina nanoparticles (γ-Al_2O_3 NPs) has been studied in the absence (binary system) and presence (ternary system) of previously sorbed Fe^{2+} as a reducing agent. In the binary system, γ-Al_2O_3 NPs sorb up to 6.5% of Tc from solution as Tc(VII). In the ternary system, the presence of previously sorbed Fe^{2+} on γ-Al_2O_3 NPs significantly enhances the uptake of Tc from pH 4 to pH 11. Under these conditions, the reaction rate of Tc increases with pH, resulting in a complete uptake for pHs > 6.5. Redox potential (Eh) and X-ray photoelectron spectroscopy (XPS) measurements evince heterogeneous reduction of Tc (VII) to Tc(IV). Here, the formation of Fe-containing solids was observed; Raman and scanning electron microscopy showed the presence of $Fe(OH)_2$, Fe(II)-Al(III)-Cl layered double hydroxide (LDH), and other Fe(II) and Fe(III) mineral phases, e.g. Fe_3O_4, FeOOH, Fe_2O_3. These results indicate that Tc scavenging is predominantly governed by the presence of sorbed Fe^{2+} species on γ-Al_2O_3 NPs, where the reduction of Tc(VII) to Tc(IV) and overall Tc retention is highly improved, even under acidic conditions. Likewise, the formation of additional Fe solid phases in the ternary system promotes the Tc uptake via adsorption, co-precipitation, and incorporation mechanisms.

* Corresponding authors.
E-mail addresses: n.mayordomo-herranz@hzdr.de (N. Mayordomo), k.mueller@hzdr.de (K. Müller).

1. Introduction

Technetium is the lightest element on the Periodic Table to be constituted solely of radioactive isotopes. Because it only occurs naturally in ultra-trace quantities, its artificial emission into the environment is of radioecological concern (Meena and Arai, 2017). The isotope ^{99}Tc is a β^- emitter with a long half-life ($t_{1/2}$ = $2.1{\cdot}10^5$ years) and represents 90% of the introduced Tc in the ecosystem (Johannsen and Spies, 1996). Historically speaking, ^{99}Tc release in the environment has been attributed to various anthropogenic sources: radiopharmacies, nuclear weapons testing, and nuclear fuel reprocessing; the latter being responsible for the majority of ^{99}Tc discharged into the ocean (Meena and Arai, 2017). Whereas some of these activities no longer occur, or are now much more regulated, others, such as the release of ground-state ^{99}Tc resulting from medical diagnostic imaging procedures, are still allowed with low restrictions. Alternative reprocessing and waste disposal schemes have addressed this issue, where ^{99}Tc is separated and then integrated into a robust matrix material for its final disposition. In order to ensure a safe storage of such materials, for example in the suggested multi-barrier nuclear waste repository (Sellin and Leupin, 2014), the Tc interaction with the repository and its environment must be understood (Ma et al., 2019). A possible ingress of water into the containment system, considered as one of the worst-case scenarios, could promote steel canister corrosion, and thus eventual radionuclide emission into the groundwater. As consequence, released ^{99}Tc might be distributed into the ecosphere, entering the food chain (Meena and Arai, 2017). In the human body, Tc can accumulate in the thyroid and the digestive system and cause dramatic health problems (EPA, 2002). In order to prevent and/or remediate existing Tc pollution, Tc scavenging materials have to be studied for their application under these settings.

Most of the reported Tc removal studies are based on the different chemical behavior manifested from its oxidation states. Tc has an assortment of oxidation states (from +VII to -I), although Tc(VII) and Tc(IV) are the most predominant under oxidizing and reducing conditions, respectively. Tc(VII), found as dissolved TcO_4^-, is considered relatively inert and highly mobile in groundwater. In contrast, Tc(IV) forms the hardly soluble TcO_2 that exhibits limited mobility. Hence, reduction of Tc(VII) to Tc(IV) offers great potential for Tc immobilization.

Lieser and Bauscher reported that Fe^{2+} is a good Tc(VII) reducing agent under anaerobic conditions (Lieser and Bauscher, 1987). However, Cui and Eriksen proved years later that Tc(VII) reduction by dissolved Fe^{2+} was kinetically hindered, despite being thermodynamically favorable, and that Tc(VII) reduction only occurs when Fe^{2+} is sorbed either on formed precipitates ($FeCO_3$ and $Fe(OH)_2$) or the surface of a substrate, also known as heterogeneous reduction (Cui and Eriksen, 1996a). In addition to these studies, Zachara et al. showed that the Tc(VII) reduction kinetics by dissolved Fe^{2+} is dependent on the Fe^{2+} concentration, being drastically faster when Fe^{2+} concentrations are higher than 0.2 mM at pH 7 (Zachara et al., 2007). They concluded that for high Fe concentrations, precipitates were formed and the heterogeneous reduction led to a faster Tc(VII) removal from solution.

Other works reported the scavenging of aqueous Tc(VII) by Fe(II)-minerals, such as siderite ($FeCO_3$) (Kobayashi et al., 2013), magnetite ($Fe(II)Fe(III)_2O_4$) (Geraedts and Maes, 2008; Cui and Eriksen, 1996b), green rust (Fe(II)-Fe(III) layered double hydroxide, LDH) (Pepper et al., 2003), $Fe(OH)_2$ (Saslow et al., 2018; Saslow et al., 2017) or mackinawite (FeS) (Liu et al., 2008). As well, some works have studied the heterogenous reduction of Tc(VII) with sorbed Fe^{2+} on minerals phases such as: goethite (α-FeOOH) (Um et al., 2011; Peretyazhko et al., 2008a), hematite (α-Fe_2O_3) (Peretyazhko et al., 2008a), corundum (α-Al_2O_3) and diaspore (α-AlOOH) (Peretyazhko et al., 2008b).

Recently, the use of nanoparticles (NPs) as sorbents has gained more attention throughout different industries and applications. For example the use of nano-sized TiO_2 (Moreno Gil et al., 2019), α-Al_2O_3 (Kadarisman et al., 2018), and/or ZrO_2 (Marlina et al., 2017) have been proposed as column matrices for ^{99}Mo/^{99m}Tc radiopharmaceutical generators as a means for chromatographically separating transmuted $^{99m}TcO_4^-$ from $^{99}MoO_4^{2-}$. Likewise, NPs also present good removal yields in the field of decontaminating pollutants, such as heavy metals (Liu et al., 2018); hence, some authors have studied Tc uptake using, for example, tin aluminum phosphate nanocomposite (Levitskaia et al., 2016) or pyrite (FeS_2) (Huo et al., 2017). However, in most studies, Tc removal is limited to a certain pH value or to a very narrow pH range – generally alkaline. Considering this, γ-Al_2O_3 NPs have been shown to be good anion sorbents in a wide pH range, as their point of zero charge is around pH 9 (Missana et al., 2014). Furthermore, γ-Al_2O_3 NPs are able to sorb Fe^{2+} on their surface (Nano and Strathmann, 2006) and promote faster Fe^{2+} oxidation (Chen and Thompson, 2018). Therefore, we hypothesize that Tc(VII) interaction on the interphase would be carried by (1) sorption on the NPs and (2) reduction to Tc(IV) by Fe^{2+} previously sorbed on γ-Al_2O_3 NPs. The latter might be an optimal process for achieving high Tc removal at the solid-solution interface in a wider pH range than the often-reported alkaline conditions.

Therefore, in this work we study the Tc removal efficiency in a wide range of pH values by γ-Al_2O_3 NPs in the absence and presence of sorbed Fe^{2+}, to combine the high removal properties of NPs with the reducing properties of sorbed Fe^{2+}. Batch contact experiments were performed in series of various pH values and ionic strengths. Additionally, the oxidation state(s) of Tc were carefully monitored using X-ray photoelectron spectroscopy to determine the presence and relative yield of Tc reduction in each sample. Finally, the formed Fe-minerals as result of the Fe^{2+} interaction with γ-Al_2O_3 NPs and of the Tc reduction were also characterized by Scanning Electron Microscopy (SEM), Raman spectroscopy and X-ray diffraction to generate a broad understanding of the governing factors of Tc retention by these systems.

2. Materials and methods

2.1. Materials and general experimental conditions

The gamma alumina nanoparticles, γ-Al_2O_3 NPs, (> 99%, Aldrich) with a nominal diameter < 50 nm were previously characterized by their isoelectric point (pH_{IE} 9), point of zero charge (pH_{PZC} 9) and N_2 BET (127 $m^2{\cdot}g^{-1}$) (Mayordomo et al., 2018).

The Fe(II)-Al(III)-Cl layered double hydroxide (LDH) synthesis is detailed in the supplementary material (S) S1.

All sorption experiments and UV–vis measurements were carried out in a glove box with N_2 atmosphere (O_2 < 0.5 ppm). All solutions and suspensions were prepared in degassed Milli-Q water (resistivity = 18.2 MΩ cm, Water Purified®), except for the $FeCl_2{\cdot}4H_2O$ solution (> 99%, Fluka), which was prepared in 0.1 M HCl to obtain 2 mM $FeCl_2$ stock solutions. The pH was measured after calibration (pH 4–9) of the electrode (semi micro, WTW). The pH of suspensions and solutions was adjusted by addition of NaOH or HCl (0.02 to 0.2 M). Redox potentials were measured after verifying the functionality of the electrode (platinum electrode with Ag/AgCl reference, Mettler Toledo Inlab redox micro 51343203) with a reference buffer (220 − 228 mV at 25 °C). The Eh values were corrected for the standard Ag/AgCl electrode (+207 mV at 25 °C).

2.2. Batch contact experiments

Contact experiments in the *binary system* were done by preparing 0.5 $g{\cdot}L^{-1}$ aqueous γ-Al_2O_3 NPs suspensions in 15 mL polypropylene tubes. The pH effect on Tc sorption was studied between pH 4.5 and 10.5 at fixed 5 μM ^{99}Tc(VII) (added as $K^{99}TcO_4$) concentration. The impact of Tc concentration on its retention was evaluated by varying it from 50 nM to 250 μM in suspensions at pH 4.5 and 0.01 M NaCl (> 99.5%, Carl Roth). After seven days of continuous shaking, samples were centrifuged at 600 x g for 1 h. The supernatant was analyzed for

pH and Eh as well as Tc concentration by liquid scintillation counting (LSC) as described below.

To investigate Tc retention on γ-Al_2O_3 NPs in the presence of Fe^{2+} (*ternary system*), a similar procedure as reported by Peretyazhko et al. (2008b) was used. In short, 0.5 g·L^{-1} γ-Al_2O_3 NPs suspensions were prepared in 60 μM $FeCl_2$ solution at fixed pH. After two days equilibration, ^{99}Tc(VII) was added to the suspension to yield a final concentration of 5 μM (more details in S2). Two samples of the suspension were taken at different points in time. One aliquot was centrifuged, and its supernatant was analyzed for Tc and Fe^{2+} concentration, as described below, as well as pH and Eh. The second aliquot was acidified with 6 M HCl to re-dissolve the sorbed Fe^{2+} and highly soluble Fe(II) precipitates. After 1 h in contact, the suspension was centrifuged, and the supernatant was analyzed for Fe^{2+} concentration – this value is hereafter referred to as Fe^{2+} after re-dissolution. For comparison, blanks were analyzed in parallel, where the concentration of dissolved Fe^{2+} was determined in the supernatant, and the concentration of sorbed Fe^{2+} was measured post-dissolution, as described above.

2.2.1. Quantification of Tc in solution

An aliquot (0.25 mL) of the supernatant was mixed with 5 mL of scintillation cocktail (Ultima Gold™, Perkin Elmer) and measured in a liquid scintillation counter (Wallac 1414, Perkin Elmer) to determine the amount of ^{99}Tc in solution.

The uptake of Tc from solution was calculated as percentage and distribution coefficient (K_D):

$$\%Tc_{retention} = \frac{([Tc]_0 - [Tc]_t)}{[Tc]_0} \times 100 \quad (1)$$

$$K_D = \frac{([Tc]_0 - [Tc]_t)}{[Tc]_t} \times \frac{V}{m} \quad (2)$$

where $[Tc]_0$ is the initial Tc concentration in the system (in Bq·mL^{-1}), $[Tc]_t$ is the concentration of Tc remaining in solution (in Bq·mL^{-1}) after certain contact time (t), V is the volume of suspension (in mL) and m is the mass of γ-Al_2O_3 NPs (in g).

2.2.2. Quantification of Fe^{2+}

The concentration of Fe^{2+} was selectively measured by UV–vis spectroscopy (TIDAS 100 J and M analytic AG) after complexation with ferrozine (Sigma Aldrich) at 562 nm as described by Stookey et al. (Stookey, 1970). An aliquot (0.25 mL) of solution was mixed with 2 mL of ferrozine stock solution (1 g·L^{-1} in 50 mM HEPES buffer, pH 7) and transferred into a quartz cuvette of 1 cm path length. Ten spectra were averaged per measurement. The aqueous Fe^{2+} molar concentration was quantified by using the Lambert-Beer equation, applying ε = 27,900 M^{-1} ·cm^{-1}. The amount of Fe^{2+}, either in solution or after re-dissolution, was recalculated using the equation:

$$\%Fe^{2+}_{aq} = \frac{[Fe^{2+}]_t}{[Fe^{2+}]_0} \times 100 \quad (3)$$

where $\%Fe^{2+}_{aq}$ represents the percentage of aqueous Fe^{2+}, $[Fe^{2+}]_0$ is the initial Fe^{2+} concentration in the system (60 μM) and $[Fe^{2+}]_t$ is the molar concentration of Fe^{2+} in solution or re-dissolved after a certain contact time (t). The concentrations of Fe^{2+} in the blank solution (re-dissolved and in solution) are presented as an average of both, since they did not differ significantly.

2.3. Speciation calculations

Calculations were carried out using the code CHESS v2.4 (van der Lee and de Wint, 1999). Speciation of Fe was carried out using the latest Fe thermodynamic database from the OECD/NEA (Lemire et al., 2013), amended with the formation constant of $Fe(OH)_2$ (Brown and Ekberg, 2016); likewise, Tc speciation was determined using the most recent thermodynamic database reported (Guillaumont et al., 2003).

Table 1
Samples measured by scanning electron microscopy (SEM) and energy-dispersive X-ray spectroscopy (EDXS).

Sample	Conditions
a	0.5 g·L^{-1} γ-Al_2O_3 suspension at pH 9
b	60 μM $FeCl_2$ at pH 9
c	synthetic Fe(II)-Al(III)-Cl layered double hydroxide (LDH)
d	0.5 g·L^{-1} γ-Al_2O_3 suspension in contact with 60 μM $FeCl_2$ at pH 9.5
e	0.5 g·L^{-1} γ Al_2O_3 suspension in contact with 5 mM $FeCl_2$ and 0.5 mM Tc(VII) at pH 9.5

2.4. X-ray photoelectron spectroscopy (XPS)

The amount of Fe^{2+} and Tc(VII) was increased in this experiment to ensure the presence of a minimum of three atoms of Tc per nm^2, which is the threshold required by the technique. A 0.5 g·L^{-1} γ-Al_2O_3 NPs suspension was in contact with 5 mM $FeCl_2$ for two days at pH 9.5, after which, Tc(VII) was added into the system to reach 0.5 mM.

For sample preparation, a drop of each suspension was dispersed on pyrolytic graphite under anoxic conditions and moved by use of a transfer vessel into the XPS (ULVAC-PHI VersaProbe II) without air contact. Spectra were acquired by monochromatic Al Kα (1486.7 eV) X-ray excitation. The elemental lines were charge referenced to C 1s (C_xH_y) at 284.8 eV.

2.5. Scanning electron microscopy (SEM), transmission electron microscopy (TEM) and energy-dispersive X-ray spectroscopy (EDXS) measurements

SEM and EDXS analyses of the samples (Table 1) were performed using two different instruments.

Samples (a–d) were isolated from the batch contact experiments. The samples were prepared by drying 20 μL of suspension on a silicon wafer under N_2 atmosphere. SEM (S-4800, Hitachi) analyses were performed at an accelerating voltage of 10 kV in conjunction with EDXS using a conventional Si(Li) detector with super ultrathin window (INCA, Oxford Instruments) attached to the SEM.

An aliquot of sample (e) was prepared for XPS, and subsequently analyzed by SEM (650, FEI Quanta FEG) operated at an accelerating voltage of 30 kV and combined with EDXS (UltraDry detector, Thermo Fisher Scientific EDX).

TEM was used to analyze the morphology and microstructure of γ-Al_2O_3 NPs. The sample was prepared by depositing a drop of a γ-Al_2O_3 NPs suspension (in deionized water) over a carbon-coated copper grid (400 mesh, S 160, Plano GmbH) and drying it under ambient conditions.

Bright-field TEM images were collected on an image-C_s-corrected transmission electron microscope (Titan 80–300, FEI) operated at 300 kV. Selected-area electron diffraction (SAED) patterns were acquired from the corresponding particle region. High-angle annular dark-field scanning transmission electron microscopy (HAADF-STEM) imaging and spectrum imaging analysis based on EDXS were performed with an electron microscope (Talos F200X, FEI) equipped with an X-FEG electron source and a Super-X EDXS detector system at an accelerating voltage of 200 kV. Prior to TEM/STEM analysis, the specimen mounted in a high-visibility low-background holder was placed for 2 s into a plasma cleaner (Model 1020, Fischione) to remove possible contamination.

2.6. Raman microscopy

Raman microscopy (Aramis, Horiba) was used to probe the resulting precipitates after the batch sorption experiments. The conditions of the measured samples are shown in Table 2.

Samples were prepared in an anoxic glove box by evaporating a 20 μL aliquot on CaF_2 glass; the sample and glass were supported in a

Table 2
Samples measured by Raman microscopy.

Sample	Conditions
1	γ-Al_2O_3 powder
2	60 μM $FeCl_2$ at pH 9.5
3	synthetic Fe(II)-Al(III)-Cl layered double hydroxide (LDH)
4	0.5 $g{\cdot}L^{-1}$ γ-Al_2O_3 suspension in contact with 60 μM $FeCl_2$ at pH 9.5
5	0.5 $g{\cdot}L^{-1}$ γ-Al_2O_3 suspension in contact with 5 μM Tc(VII) at pH 4.5, 6.5 and 9.5
6	0.5 $g{\cdot}L^{-1}$ γ-Al_2O_3 suspension in contact with 5 mM $FeCl_2$ and 0.5 mM Tc(VII) at pH 6.5 and 9.5

polyoxomethylene container enclosed by a CaF_2 window (Figure S3), which ensured anoxic conditions during the measurement. The spectra were recorded using a 532 nm laser (50 mW) with a 10-fold objective and no filter, a pin-hole of 300 μm and a slit of 300 μm. The spectra were taken as an average of three scans of 10 s, in which the laser exposure to the sample was minimized to avoid degradation. The intense band shown at 321 cm^{-1} belongs to CaF_2.

2.7. X-ray diffraction (XRD)

XRD (MiniFlex 600 powder XRD, Rigaku with an X-ray source of Cu Kα) was used to identify the solids formed after reacting with Fe^{2+} and Tc in batch contact experiments. More information about the measured samples can be found in S3.

3. Results

3.1. Tc(VII) sorption on γ-Al_2O_3: the binary system

The surface complexation of Tc(VII) on γ-Al_2O_3 has been analyzed as a function of pH and TcO_4^- concentration. Shown in Fig. 1a, the TcO_4^- sorption on γ-Al_2O_3, although initially low, i.e., < 10%, decreases with increasing pH, primarily between pH ≈ 7-8. This behavior is attributed to the diminishing positive surface charge on the γ-Al_2O_3 (pH_{IE} 9) surface with increasing basicity of the solution. However, the isotherm plot at pH = 4.5 (Fig. 1b) shows a linearly increasing trend, with a slope of 1.04 ± 0.03 (r = 0.996), which implies that surface complexation occurs at a single site on the γ-Al_2O_3. The maximum TcO_4^- sorption occurs under acidic conditions, with an average value of 6.5% (K_D ≈ 0.14 $mL{\cdot}g^{-1}$), which is consistent with previously reported results of Tc interaction with high-surface area γ-Al_2O_3 (Kumar et al., 2011).

3.2. Tc uptake by γ-Al_2O_3 in presence of Fe^{2+}: ternary system

3.2.1. Effect of pH, ionic strength and time on the Tc removal

For a better comparison with the results of the binary system, experiments were performed as a function of pH at two ionic strengths for 7 and 30 days. Firstly, the Fe^{2+} sorption on γ-Al_2O_3 was studied for better understanding its effect on Tc retention in the ternary system. The measured Fe^{2+} concentration in solution and after re-dissolution in the batch experiments is plotted in Figure S4 (supplementary material). It is observed that Fe^{2+} content in solution and after re-dissolution decrease with increasing pH at both ionic strengths, where the amount of Fe^{2+} after re-dissolution is higher than Fe^{2+} in solution. The difference between both measured Fe^{2+} concentrations could correspond either to Fe^{2+} sorbed on the γ-Al_2O_3 and/or to the formation of soluble Fe(II)-minerals. The concentration of Fe^{2+} after re-dissolution is lower than 75% of initial Fe^{2+} for pH > 6.5 at both ionic strengths. In contrast, for pH < 6.5 the aqueous Fe^{2+} concentration decreases by 10%, but only in the water system (Figure S4a).

Fig. 2 depicts the Tc removal in the ternary system. The Tc uptake increases with increasing pH at both ionic strengths, being complete for pH > 6.5; this trend is typically expected for cation sorption on metal oxides as the surface charge becomes more negative with increasing pH (Dzombak and Morel, 1990). However, Tc retention increases with decreasing ionic strength at pH < 6, while its sorption behavior is independent of ionic strength at pH > 6. A faster kinetic Tc uptake is also observed at pH < 6 in water, increasing from 20% (K_D ≈ 550 $mL{\cdot}g^{-1}$) to 40% (K_D ≈ 1100 $mL{\cdot}g^{-1}$) of Tc removal after 7 and 30 days of contact, respectively. The Tc scavenging efficiency of the ternary system is higher than the one reported for Tc(IV) sorption on γ-Al_2O_3 (Kumar et al., 2011), whose maximum Tc(IV) retention (30%) occurred in the pH range from 6 to 8.

The Pourbaix diagram (Fig. 2c) was calculated considering the Tc(VII)/Tc(IV) redox-couple equation given in (Meyer et al., 1991). It shows that the measured Eh values for most of the experimental data lie on the stability region of Tc(IV), which indicates that Tc retention in the ternary system is a consequence of Tc(VII) reduction. Nevertheless, to corroborate the oxidation state of the Tc in the ternary system, XPS experiments were carried out (Figure S5). The spectrum shows two Tc 3d peaks, $3d_{3/2}$ and $3d_{5/2}$, where the binding energy of $3d_{5/2}$ is 256.4 eV. This energy value indicates that Tc is present in the +4 oxidation state in the sample (Wester et al., 1987), confirming Tc(VII) reduction. In addition, XPS shows the presence of Fe(II) on the surface.

3.2.2. Detailed kinetics of Fe^{2+} evolution and Tc uptake

Further experiments were performed to better elucidate the Tc scavenging kinetics in the ternary system at pH 4.8, 7.0 and 9.5 in water. Fig. 3(a–c) represent the evolution of Fe^{2+} concentration in the

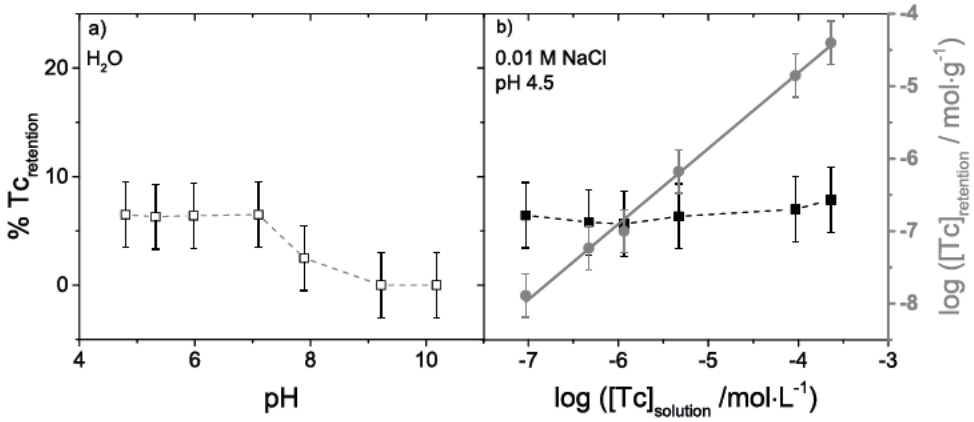

Fig. 1. (a) Tc ($[Tc(VII)]_0$ = 5 μM) retention on 0.5 $g{\cdot}L^{-1}$ γ-Al_2O_3 as a function of pH in H_2O and (b) [Tc(VII] at pH 4.5 and 0.01 M NaCl (colours according to labels of the ordinate). Dashed lines are shown to guide the eye.

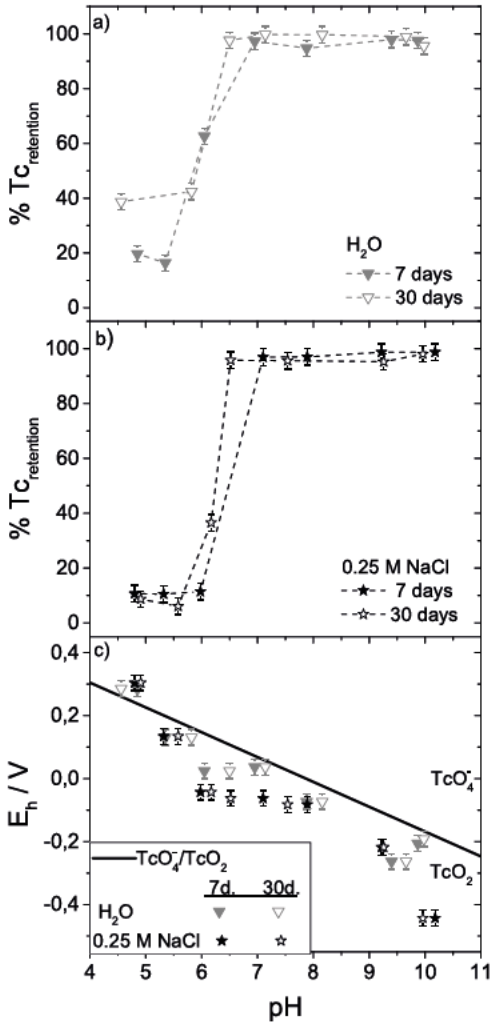

Fig. 2. Tc ([Tc(VII)]$_0$ = 5 μM) retention by 0.5 g·L^{-1} γ-Al_2O_3 containing sorbed Fe^{2+} ([Fe^{2+}]$_0$ = 60 μM) as a function of pH in (a) H_2O and (b) 0.25 M NaCl after 7 and 30 days of contact. (c) Measured redox potential (Eh) as a function of pH for the samples plotted in (a) and (b) and calculated equilibrium line between TcO_4^- and TcO_2 according to (Meyer et al., 1991). Dashed lines are shown to guide the eye.

ternary system and in a blank solution, and Fig. 3(d–e) shows the amount of Tc removed from solution.

Fig. 3(a–c) shows that Fe^{2+} concentration changes with time at different pH values. It is evident that a faster decrease of aqueous Fe^{2+} is observed with increasing pH. At pH 4.8 (Fig. 3a), the amount of Fe^{2+} in solution and after re-dissolution in the ternary system only slightly decreases with increasing contact time (as observed in the Figure S4), and the Fe^{2+} concentration in the blank solution is barely affected over the observed period. At pH 7.0 (Fig. 3b), the Fe^{2+} concentration in solution is lower than after re-dissolution and follows the same trend as observed in Figure S4, while the kinetic decrease of dissolved Fe^{2+} could be related to the higher Fe^{2+} sorption on γ-Al_2O_3, as reported by Nano and Strathmann (2006). At pH 9.5, the Fe^{2+} concentrations decrease below the detection limit for both the Fe^{2+} in solution in the ternary system and in the blank; however, it was possible to measure Fe^{2+} after re-dissolution due to sorbed Fe^{2+} being liberated from the γ-Al_2O_3. This trend was also observed in an additional Fe^{2+} sorption experiment performed with γ-Al_2O_3 for longer time (S4 and Figure S6). The Fe(II) speciation was calculated to explain the depletion of Fe^{2+} in the blank solution at pH 9.5 (Figure S7). According with the calculation, for pH > 8, the main chemical species is solid $Fe(OH)_2$, with a solubility constant of log K_{sp} = −12.25 (Brown and Ekberg, 2016); this is a clear indication why it is not possible to detect Fe^{2+} in the blank solution. In addition, the X-ray diffractogram of the precipitate resulting from a Fe^{2+} solution at pH 9.5 coincides with the diffractograms of both $Fe(OH)_2$ from the International Center for Diffraction Data (ICDD) (ICDD 01-081-8012) and NaCl (ICDD 010-005-0628) (Figure S8).

Fig. 3(d–e) shows that the Tc removal is faster with increasing pH. Complete Tc removal was achieved after seven days at pH 7 and after one day at pH 9.5. At pH 4.8, an increase of Tc uptake is observed among 7 and 15 days of contact, as previously observed in Fig. 2a.

Furthermore, it is noteworthy that the formation of a solid was visible to the naked eye during the two days of Fe^{2+} pre-sorption on γ-Al_2O_3 at pH 9.5 and pH 7.0, even in the absence of Tc, which was especially pronounced at alkaline conditions. This solid was also observed after Tc addition. According to Elzinga (2012), Fe^{2+} and γ-Al_2O_3 form a Fe(II)-Al(III) layered double hydroxide (LDH) under circumneutral to alkaline pH, whose solubility is very low, $K_{sp} \approx 10^{-21}$ (Bhattacharya and Elzinga, 2018). In this case, Fe(II)-Al(III)-Cl LDH would be formed due to the presence of Cl^- (i.e. the addition of $FeCl_2$). In addition to the predicted formation of $Fe(OH)_2$ and Fe(II)-Al(III)-Cl LDH, a change of color from white to brown was observed in the ternary system with increasing pH, likely an indication for the precipitation of other iron secondary phases.

3.2.3. Identification of the formed Fe precipitates

In an attempt to identify the solids generated in this process, speciation calculations, SEM/EDXS analyses and Raman measurements were performed.

3.2.3.1. Speciation. The reduction potential for Fe^{3+}/Fe^{2+} is 0.772 ± 0.002 V (Lemire et al., 2013). In contrast, the Tc(VII)/Tc(IV) reduction couple depends highly on the Tc(IV) formed species. The calculated potential for the reduction of TcO_4^- to $TcO_2{\cdot}1.6H_2O$ is 0.746 ± 0.004 V in pure water, but it could be even higher, e.g., ~0.844 V, in 1.3 M Cl^- solutions (Guillaumont et al., 2003). Considering these values, the formation of Fe^{3+} is possible due to the reduction of Tc(VII) to Tc(IV) in this system, and consequently also the formation of Fe(III) solids and/or Fe(II)/Fe(III) solids is possible (Jolivet et al., 2006; Usman et al., 2018).

In order to predict which Fe-minerals could be formed in the ternary system, Tc and Fe speciation was calculated accounting for the initial Tc (VII) and Fe^{2+} concentrations used in the experimental conditions (Figure S9). The resulting data have to be evaluated carefully, as the code assumes that Tc is homogenously reduced and predicts the total Tc reduction at pH 4.5 (Figure S9b). Nevertheless, both assumptions are incorrect. The Tc reduction in the ternary system described here cannot be accurately calculated since the reduction potential of sorbed Fe^{2+} on minerals is different than the one in solution, which has been previously observed for Fe^{2+} sorbed on Fe(III) minerals (Gorski et al., 2016), γ−Al_2O_3 (Li et al., 2009) and TiO_2 (Zhu et al., 2013). Additionally, the homogeneous reduction of Tc(VII) by Fe^{2+} is a thermodynamically favorable process, but it is kinetically hindered (Cui and Eriksen, 1996b). Therefore, the calculations can only be used to analyze the feasibility of Fe-mineral formation.

Figure S9a shows that the dissolved Fe^{3+} could form hematite (Fe_2O_3) under circumneutral to acidic pH and magnetite ($Fe(II)Fe(III)_2O_4$) under circumneutral to alkaline pH. Considering the predicted and reported formation of Fe-minerals, including the Fe(II)-Al(III)-Cl LDH phase at circumneutral to alkaline pH, a very complex mixture of minerals can be expected to form in the ternary system, which might also contribute to the Tc sequestration by other mechanisms, such as co-precipitation.

3.2.3.2. Scanning electron microscopy combined with energy-dispersive X-ray spectroscopy. SEM imaging (Fig. 4) combined with EDXS analysis (from Figure S10 to Figure S13) was applied to identify the morphology

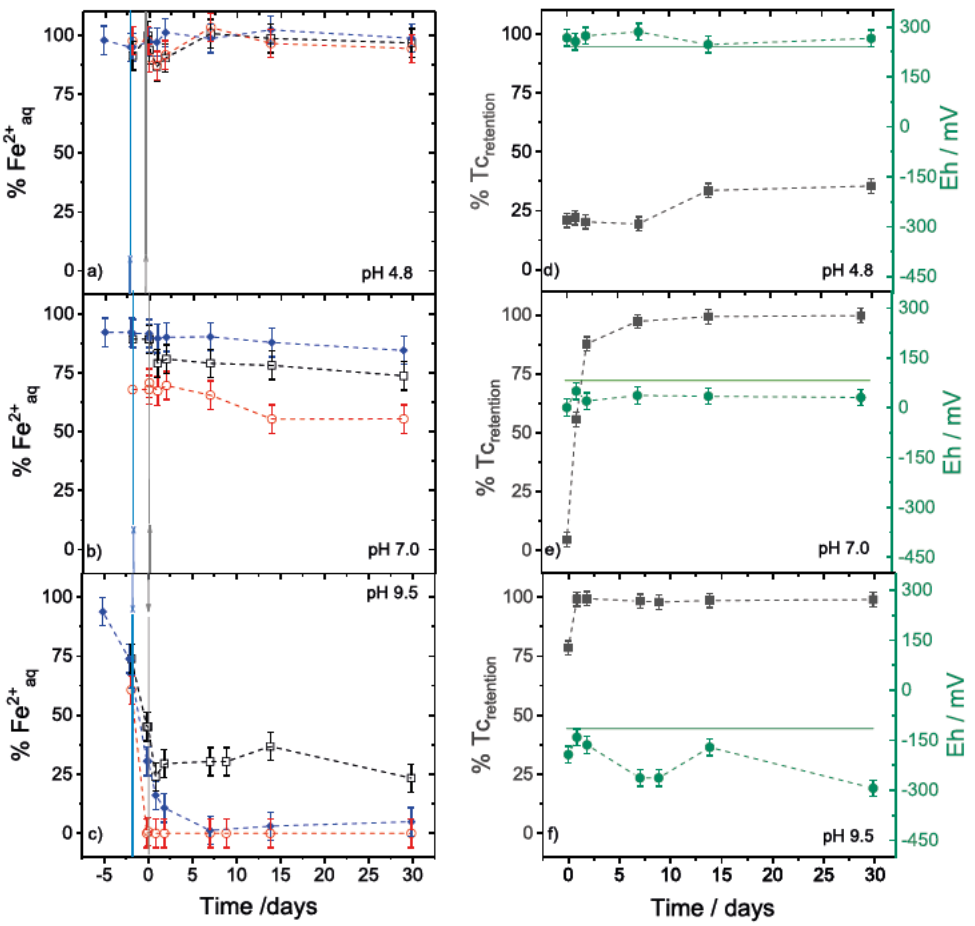

Fig. 3. Plots of batch experiments after Tc([Tc(VII)]$_0$ = 5 μM]) has been in contact with 0.5 g·L^{-1} γ-Al_2O_3 containing sorbed Fe^{2+} ([Fe^{2+}]$_0$ = 60 μM) (ternary system) as a function of time at pH 4.8, pH 7 and pH 9.5. (a, b and c) Fe^{2+}aq measured (represented as %) (○) directly in solution of the ternary system, (□) after an aliquot of ternary system suspension has been acidified, representing the Fe^{2+} after re-dissolution and (♦) Fe^{2+} aq measured in a blank solution at the same pH cond tions. (d, e and f) (■) Percentage of aqueous Tc removed, (●) measured E_h and (solid line) calculated equilibrium line between TcO_4- and TcO_2 using (Meyer et al., 1991). Blue and grey arrows indicate the alumina and Tc addition, respectively. Dashed lines are shown to guide the eye (for interpretation of the references to colour in this figure legend, the reader is referred to the web version of this article).

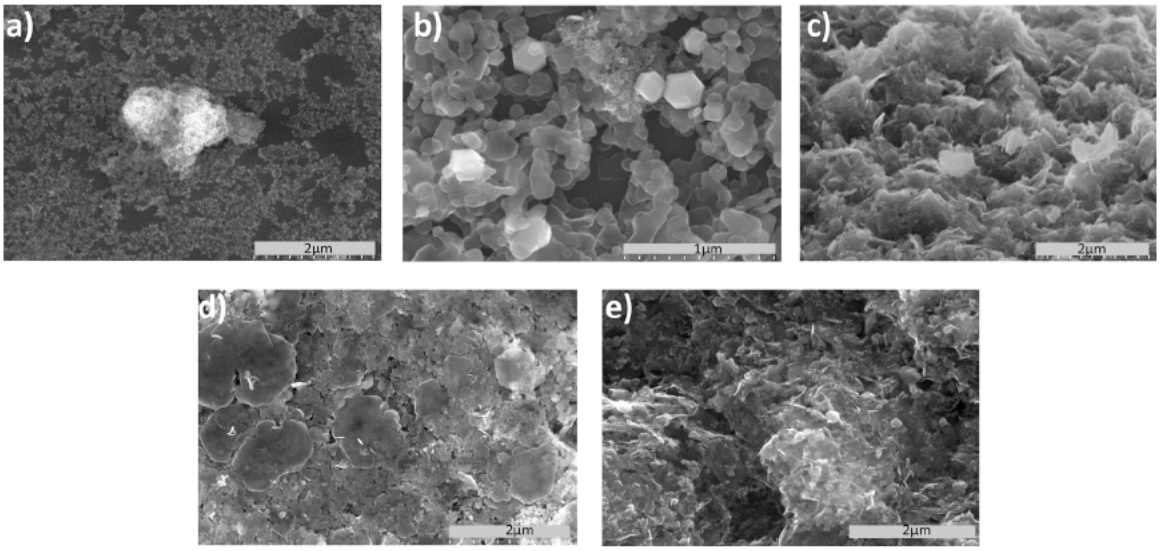

Fig. 4. Scanning electron microscopy images obtained after drying suspensions of (a) γ-Al_2O_3 at pH 9, (b) $FeCl_2$ at pH 9, (c) Fe(II)-Al(III)-Cl layered double hydroxide at pH 9, (d) γ-Al_2O_3 with sorbed Fe^{2+} at pH 9.5 and (e) γ-Al_2O_3 with sorbed Fe^{2+} after Tc(VII) contact at pH 9.5.

of the precipitates / minerals formed in the ternary system.

As shown in Fig. 4a and Figure S10, the pure γ-Al_2O_3 NPs form large aggregates, which is expected when the pH is near its pH_{IE} (Missana et al., 2014). The precipitates formed in the blank $FeCl_2$ solution at pH 9.5 exhibit different morphological features, such as prisms with hexagonal basal plane (~ 200–300 nm) and thin, irregularly shaped globules (~ 100–500 nm) (Fig. 4b and Figure S11), indicating the presence of at least two different phases. To note, the synthetic Fe(II)-Al(III)-Cl LDH forms piled thin-layered structures (~ 400–800 nm) (Fig. 4c). The solids formed after γ-Al_2O_3 was in contact with Fe^{2+} (Fig. 4d and Figure S12) show various morphologies: hexagons and globules that resemble the ones observed in Fig. 4b and c, respectively, and small spherical particles similar to the ones in Fig. 4a. These four bulk solids strongly differ with those obtained for the ternary system after Tc(VII) reduction (Fig. 4e and Figure S13), which implies that drastic mineralogical changes have occurred as result of γ-Al_2O_3

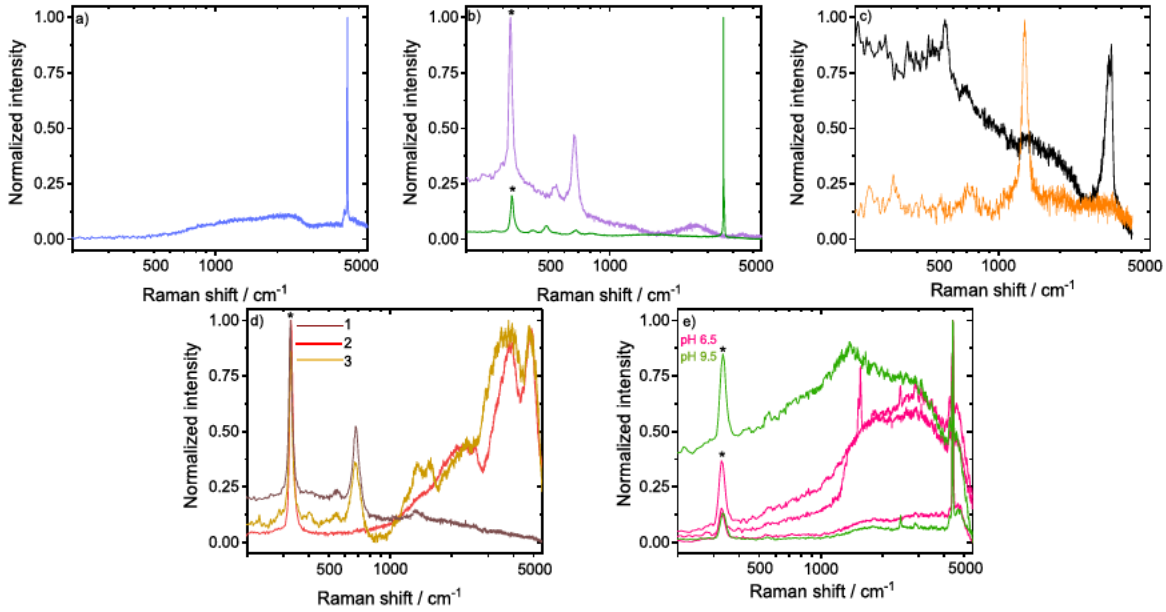

Fig. 5. Raman spectra obtained in dried suspensions of (a) γ-Al_2O_3, (b) $FeCl_2$ at pH 9, (c) Fe(II)-Al(III)-Cl layered double hydroxide (black) without and (orange) with photo-oxidation, (d) γ-Al_2O_3 with sorbed Fe^{2+} at pH 9.5 and (e) γ-Al_2O_3 with sorbed Fe^{2+} after Tc(VII) contact at pH 6.5 and 9.5. The band * corresponds to CaF_2. (For interpretation of the references to colour in this figure legend, the reader is referred to the web version of this article).

interaction with Fe^{2+} and Tc(VII). EDXS analysis of the resulting material formed in the ternary system (Figure S13) reveals that Al, Fe and Tc atoms coexist in the sample. Although no isolated Tc particles were identified, it is noted that higher Tc concentrations are measured in spots where Fe content is higher (Figure S13).

3.2.3.3. Raman microscopy. Raman microscopy was used to probe several of the collected solids previously mentioned (Fig. 5 and Figure S14). The γ-Al_2O_3 powder has a characteristic sharp peak at 4395 cm^{-1} and a broad weak peak that expands from 1100 to 2600 cm^{-1} (Fig. 5a). Fig. 5b shows two different spectra recorded for $FeCl_2$ under alkaline pH. One of the spectra shows Raman shifts at 267, 492, and 3584 cm^{-1}; the other one shows Raman shifts at 240, 294, 528, 548 and 673 cm^{-1}. In order to verify whether the formation of Fe (II)-Al(III) LDH occurs when γ-Al_2O_3 and Fe^{2+} are in contact under circumneutral to alkaline pH, they were synthesized as the pure phase in a separate set of experiments and further characterized (S2) to determine their contribution in the Raman signals (Fig. 5c). Recording the Raman spectra of the synthetic LDH was challenging due to photo-oxidation via laser irradiation– apparent from the color transformation of the ROI from light green to red observed after the measurement. The spectra recorded for the photo oxidized LDH present Raman shifts at 235, 307, and 1341 cm^{-1}, while the spectra of the LDH without photo oxidation show peaks at 280, 360, 543, 681 cm^{-1} and an intense peak characteristic in the region of 3445–3560 cm^{-1} (Fig. 5c).

The different analyzed spots of the γ-Al_2O_3 in contact with Fe^{2+} at pH 9.5 show different peaks (Fig. 5d), likely attributed to the presence of multiple phases, consistent with the microscopy. Area one shows bands at 557, 682 cm^{-1} and a small contribution at 1321 cm^{-1}. The second measured spot presents Raman shifts around 1900–2600 cm^{-1}, 3825 and 4950 cm^{-1}. The third area shows, together with the above-mentioned shifts for the spots one and two, one additional peak at 1606 cm^{-1}. The spectra obtained for γ-Al_2O_3 in the binary system with Tc show a sharp peak at 4400 cm^{-1} and a broad peak at 4700 cm^{-1} (Figure S14). In the case of the ternary system (Fig. 5e), the main bands are at 1350, 1650 and 4400 cm^{-1}, with minor bands are at around 2443, 3976 and 3146 cm^{-1} and a broad peak at around 3100 cm^{-1}.

3.2.3.4. X-ray diffraction. The diffractograms of the precipitates obtained after Fe^{2+} interaction with γ-Al_2O_3 and Tc interaction with γ-Al_2O_3 containing pre-sorbed Fe^{2+} were obtained at various pH values. In all of the cases the diffractograms fit the one registered for pure $\gamma-Al_2O_3$, whose number is ICDD 00-002-1420 (results not shown).

4. Discussion

Although in other studies γ-Al_2O_3 NPs have shown a high affinity for anions in general (Missana et al., 2014), it is not the case for Tc(VII) and the determined sorption behavior is similar to the one reported for high-surface area γ-Al_2O_3 (Kumar et al., 2011). However, despite the small fraction of Tc(VII) sorption on γ-Al_2O_3, these results should be considered in the long-term assessment of nuclear waste management, as in most cases, TcO_4^- is assumed to be a conservative tracer that has negligible mineral interaction (Lieser and Bauscher, 1987).

In comparison with the binary system, the Tc uptake in the ternary system is highly improved. The enhanced Tc removal and its faster uptake with increasing pH are related to the amount of Fe^{2+} sorbed on the γ-Al_2O_3 surface, which promotes Tc(VII) heterogeneous reduction. Likewise, the enhanced heterogeneous Tc(VII) reduction with increasing pH is due to the decrease of the Fe^{2+}/Fe^{3+} oxidation potential when Fe^{2+} is sorbed on γ-Al_2O_3 (Li et al., 2009).

In order to reduce 5 μM Tc(VII), three equivalents of Fe^{2+} (15 μM) are required, meaning that the initial 60 μM Fe^{2+} in solution would be decreased to 45 μM Fe^{2+} (representing 75% of the initial Fe^{2+}). Indeed, values below 75% Fe^{2+} concentration after re-dissolution are measured for pH > 6.5, which agree with the complete Tc uptake measured. The incomplete reduction for pH < 6.5 is likely due to the lower amount of Fe^{2+} sorbed on the γ-Al_2O_3 shown in the experiments (Fig. 3(a–c) and Figure S4), especially at short contact times and in 0.25 M NaCl, which agrees with previous studies (Nano and Strathmann, 2006). It is also noted that the potential formation of soluble Tc(IV) species, e.g., $[Tc_2O_2(OH)_2]^{2+}$, Tc(IV)-O-Cl and Tc(IV)-Cl-H_2O species, and lower oxidation states of Tc, such as Tc^{3+}, (Grambow et al., 2018; Poineau et al., 2006) at higher chloride and acid concentrations would also hinder the formation of TcO_2. Moreover, the faster Tc uptake with increasing pH is supported by the fact that the presence of γ-Al_2O_3 enhances the rate of Fe^{2+} oxidation due to a more favorable electron-

transfer environment (Chen and Thompson, 2018).

The observed higher Tc removal in pure water than in 0.25 M NaCl at acidic pH and its kinetic effect in the ternary system (Figs. 2a and 3 d) can be explained by the high sorption capability of γ-Al_2O_3, in this case for Fe^{2+}. Nano and Strathmann showed that the Fe^{2+} sorption on γ-Al_2O_3 at pH < 6 corresponds to 5–7% retention, and it slightly increases when Fe^{2+} concentration or ionic strength decreases. Additionally, they showed that Fe^{2+} retention occurred in two steps at pH 7: the first occurs within a few hours (40% retention), while the second proceeds within 8 and 33 days of contact (70% retention) (Nano and Strathmann, 2006). These observations clearly agree with the measured Fe^{2+} concentration in our system (Fig. 3(a–c) and Figure S4). This unexpected cation sorption under acidic conditions by γ-Al_2O_3 NPs has also been recently reported for Sr^{2+} (Mayordomo et al., 2019). Therefore, the good ion sorption capability of the γ-Al_2O_3 NPs is related to their small size (< 50 nm, Figure S15) and its high specific surface area (127 $m^2 \cdot g^{-1}$) and promotes a wide Fe^{2+} sorption, which strongly supports the heterogeneous Tc(VII) reduction in the ternary system.

We can identify the formed solid phases formed during the batch contact experiments of the ternary system by combining SEM/EDXS analysis results and Raman spectra. In most cases, the sensitivity of XRD was not sufficient to identify the surface formed secondary phases because they are present only in low concentrations and, therefore, could not be distinguished from the bulk material. In contrast, Raman microscopy allows focusing the laser on specific surface spots and, thus, the identification of minor solids, regardless of their low concentration. For the $FeCl_2$ solution under alkaline pH, the primary species was Fe$(OH)_2$, as speciation calculations predicted (Figure S7) and XRD showed (Figure S8). However, according to the Raman spectra and the SEM images, two different phases are present in the solid. The Raman peaks at 267, 492, and 3584 cm^{-1} (Fig. 5b) are similar to those assigned to Fe$(OH)_2$, i.e., 260, 407 and 3573 cm^{-1} (Lutz et al., 1994). SEM imaging also revealed particle morphology (Fig. 4b) consistent with that of Fe$(OH)_2$, which forms flat planes that produce a brucite-like layered structure (Jolivet et al., 2006). The second set of Raman peaks at 240, 294, 528, 548 and 673 cm^{-1} can be attributed to Fe_3O_4 (Hanesch, 2009), which is also supported by the hexagonal crystals observed in Fig. 4b) that resemble magnetite (Kimura et al., 2013). The formation of magnetite in our system indicates the presence of Fe(III) in the $FeCl_2$ stock solution.

The band observed at 3445–3560 cm^{-1} in the Fe(II)-Al(III) LDH spectra (Fig. 5c) is assigned to the OH stretching and it is in the range of other reported Raman spectra for LDH phases (Rozov et al., 2010); while its photo oxidation product is identified as hematite (Hanesch, 2009). The morphology of the resulting solid also agrees with its LDH identity, as its observed structure (Fig. 4c) resembles those of previously reported LDHs (Goh et al., 2008; Wang et al., 2013).

In the Raman spectra for the solid, resulting from the interaction of γ-Al_2O_3 and Fe^{2+} at pH 9.5, several bands are visible (Fig. 5d). The peak at 3825 cm^{-1} is related to the formation of LDH − the band shift in comparison with the ones of the Fig. 5c could be due to structural differences of the synthetic Fe(II)-Al(III)-Cl LDH and the *in situ* generated LDH after interaction of Fe^{2+} with γ-Al_2O_3. Additional bands at 557 and 682 cm^{-1} can be attributed to magnetite (Hanesch, 2009), and the small contributions at 1321 and 1606 cm^{-1} could be associated to hematite and maghemite (Hanesch, 2009), respectively, formed after photo-oxidation. Finally, the band around 1900–2600 cm^{-1} and 4950 cm^{-1} is likely associated to the γ-Al_2O_3. The latter bands are drastically shifted in comparison with the γ-Al_2O_3 powder (Fig. 5a); one feasible explanation is the variation of the γ-Al_2O_3 vibrations due to the Fe^{2+} sorption on γ-Al_2O_3. The globules present in Fig. 4d support the formation of LDH because their structure is similar to the one of the synthetic Fe(II)-Al(III)-Cl LDH (Fig. 4c).

The spectra of γ-Al_2O_3 after the reaction with Tc (Figure S14) show similarities to the spectra of γ-Al_2O_3 powder (Fig. 5a) and, due to the absence of Tc(VII) Raman shifts expected to be at 880 and 900 cm^{-1} (Weaver et al., 2017), we can only assume that the presented features at 1800, 3200 and 4700 cm^{-1} belong to the interaction of water with the alumina.

The Raman spectroscopic identification of the solid formed in the ternary system is much more difficult because the intensity resulting from the laser interaction with the sample saturates the detector. Therefore, the spectra shown in Fig. 5e were obtained after adding a filter to the laser beam; as a consequence, information about bands with lower intensity might have been lost. The spectra bands shown around 1350 and 1650 cm^{-1} could be assigned to maghemite and hematite, respectively. As well, for both pHs, the characteristic band of γ-Al_2O_3 (4400 cm^{-1}) is still present and a broad peak at around 3100 cm^{-1}, which might be attributed to a shift of the LDH band after interacting with Tc. The presence of LDH in the ternary system is supported by the arbitrary presence of small layered structures in Fig. 4e. The additional bands observed in the spectra are difficult to correlate with other species. The magnetite features shown in Figs. 4d and 5 d are not observed in Figs. 4e and 5 e, which could be due to the mineralogical change of magnetite due to Tc e.g. formation of other Fe phase or Tc incorporation. Additionally, the absence of a proper TcO_2 spectrum in the literature hinders its possible identification, so it is assumed that these signatures might be related to TcO_2 or to Tc-O bands; however, this is only a hypothesis and further experimentation is required for accurate determination. Studies have reported that Fe^{2+} oxidation in presence of alumina leads to nanocrystalline lepidocrocite (γ-FeOOH) and goethite (α-FeOOH) (Chen and Thompson, 2018), which are also likely the case here, wherein the bands shown at around 400 and 550 cm^{-1} could be related to those phases (Fig. 5e).

Although the formation of the various solid Fe phases is possible within this system, high Tc retention capabilities have been reported for most of them and, despite being present in small amounts, they can contribute to Tc retention. Tc forms surface complexes on, and is also incorporated into magnetite (Marshall et al., 2014; Yalçıntaş et al., 2016; Luksic et al., 2018), which stabilizes Tc(IV) and prevents its re-oxidation. The $Fe(OH)_2$ phase has been shown to incorporate Tc(IV) under alkaline pH (Saslow et al., 2017; Luksic et al., 2018). The resulting Fe(III) transforms into magnetite (Saslow et al., 2017), and α- and β-FeOOH (Kergourlay et al., 2018), whose formation prompts Tc co-precipitation (Luksic et al., 2018). Although Tc sorption on Fe(II)-Al(III)-Cl LDH has not yet been studied, a recent paper reports an efficient method via anion exchange of TcO_4^- by CO_3^{2-} and NO_3^- counter anions of Mg(II)-Al(III) and Mg(II)-Fe(III) LDH phases (Daniels et al., 2019). This behavior is consistent with the high anion exchange capacity of LDH phases (Goh et al., 2008). It is envisioned that this could enable the removal of unreacted TcO_4^-, as well as the retention of Tc by surface complexation, incorporation (Forano et al., 2013), or in the case of Fe(II)-Al(III)-Cl LDH, by Tc(VII) reduction. Moreover, the impossibility of measuring isolated Tc particles in the ternary system by EDXS analysis (Figure S13) supports that Tc(IV) could be related either to the surface complexes formation, incorporation, or co-precipitation with the solids in suspension. Therefore, the formation of the Fe-minerals improves the Tc retention performance of the Fe^{2+}-γ-Al_2O_3 system, and thus is an important factor to consider.

5. Conclusions and outlook

The interaction of Tc(VII) with γ-Al_2O_3-NPs (binary system) yielded a maximum of 6.5% retention under acidic conditions with little to no uptake at pH > 7. This is consistent with, and has implications for, commercial medical $^{99}Mo/^{99m}Tc$-radiopharmaceutical generators where Al_2O_3 is used as the primary column material. When Fe^{2+} is presorbed on the γ-Al_2O_3 (ternary system), Tc uptake is due to the Tc(VII) reduction to Tc(IV), which is nearly complete from neutral to basic conditions. At lower pHs Tc retention capacities are improved up to ~40%. Likewise, faster uptake kinetics of Tc for the ternary system were observed with increasing pH, showing complete Tc scavenging for

pH values higher than pH 6.5. These results indicate that ideal sorbent capabilities of γ-Al_2O_3 NPs - improved in comparison with their bulk counterparts due to their higher surface to volume ratio - govern the efficiency and rate of the heterogeneous Tc(VII) reduction in the ternary system.

Raman microscopy allowed to identify the formation of various solids in the ternary system: Fe(II)-Al(III)-Cl LDH, $Fe(OH)_2$, Fe_3O_4, FeOOH and Fe_2O_3. Their presence could improve the Tc retention, despite their low concentrations. The interactions of Tc with $Fe(OH)_2$, Fe_3O_4, FeOOH and Fe_2O_3 have been already published; however, the retention of Tc by the Fe(II)-Al(III)-Cl has not yet been reported, and should be investigated in more detail as it seems to be a promising candidate to remove Tc.

Ultimately, the results presented here show that Fe^{2+} sorbed on γ-Al_2O_3 is an efficient Tc scavenging material, particularly under anoxic, basic conditions where uptake is complete. These findings have implications related to the construction and operation of geological repositories, where similar environmental conditions will likely occur. Likewise, the interaction of Fe, arising from omnipresent Fe-based materials, such as steel and other structural / construction components, and their inevitable corrosion products, with minerals in the host rock, such as γ-Al_2O_3, or those that chemically resemble it, e.g., zirconia, titania, etc., should be accounted for when developing multisystem models for predicting Tc behavior under these settings. However, for building up a reliable model that represents the Tc uptake by γ-Al_2O_3 in the ternary system, it is required to decipher the responsible mechanisms within surface complexes formation, incorporation, or co-precipitation with the solids in suspension.

Author contribution

Natalia Mayordomo designed the experiments, performed the sorption experiments, carried out the modeling, synthesized the Fe(II)-Al(III)-Cl LDH, prepared the samples for XPS, Raman microscopy, SEM microscopy, and XRD, assisted with Raman microscopy measurements, interpreted the data and wrote the original draft of the manuscript.

Diana M. Rodríguez contributed to sorption experiments and sample preparation for XRD and XPS and contributed to the revision of the original manuscript.

Dieter Schild performed the XPS measurements and their data interpretation and contributed to the revision of the original manuscript.

Konrad Molodtsov assisted with Raman microscopy measurements and their data interpretation, designed the Raman cell and contributed to the revision of the original manuscript.

Erik V. Johnstone contributed to the writing of the original draft of the manuscript.

Salim Shams Aldin Azzam performed the XRD measurements and data interpretation.

René Hübner performed the SEM and TEM measurements, their data interpretation and contributed to the revision of the original manuscript.

Vinzenz Brendler supervised and contributed to writing the manuscript.

Katharina Müller supervised and contributed to writing of the manuscript.

Declaration of Competing Interest

The authors declare that they have no known competing financial interests or personal relationships that could have appeared to influence the work reported in this paper.

Acknowledgments

This work has been developed in the frame of the VESPA II project (02E11607B), supported by the German Federal Ministry of Economic Affairs and Energy (BMWi). We acknowledge E. Christalle for the SEM and EDXS measurements, A. Ikeda and K. Heim for the LDH XRD measurement, D. Falkenberg for the elaboration of the Raman cells, S. Weiss and C. Müller for their support in the laboratory and S. Henke for keeping the glove box in perfect condition.

Appendix A. Supplementary data

Supplementary material related to this article can be found, in the online version, at doi:https://doi.org/10.1016/j.jhazmat.2020.122066.

References

Bhattacharya, L., Elzinga, E.J., 2018. A comparison of the solubility products of layered Me(II)– Al(III) hydroxides based on sorption studies with Ni(II), Zn(II), Co(II), Fe(II), and Mn(II). Soil Syst. 2, 1–15. https://doi.org/10.3390/soilsystems2020020.

Brown, P.L., Ekberg, C., 2016. Hydrolysis of Metal Ions Vol 2. Wiley-VCH, Weinheim (Germany).

Chen, C., Thompson, A., 2018. Ferrous Iron oxidation under varying pO_2 levels: the effect of Fe(III)/Al(III) oxide minerals and organic matter. Environ. Sci. Technol. 52, 597–606. https://doi.org/10.1021/acs.est.7b05102.

Cui, D., Eriksen, T.E., 1996a. Reduction of pertechnetate by ferrous iron in solution: influence of sorbed and precipitated Fe(II). Environ. Sci. Technol. 30, 2259–2262. https://doi.org/10.1021/es9506263.

Cui, D., Eriksen, T.E., 1996b. Reduction of pertechnetate in solution by heterogeneous electron transfer from Fe(II)-containing geological material. Environ. Sci. Technol. 30, 2263–2269. https://doi.org/10.1021/es950627v.

Daniels, N., Franzen, C., Murphy, G.L., Kvashnina, K., Petrov, V., Torapava, N., Bukaemskiy, A., Kowalski, P., Si, H., Ji, Y., Hölzer, A., Walther, C., 2019. Application of layered double hydroxides for ^{99}Tc remediation. Appl. Clay Sci. 176, 1–10. https://doi.org/10.1016/j.clay.2019.04.006.

Dzombak, D.A., Morel, F.M.M., 1990. Surface Complexation Modeling. Hydrous Ferric Oxide, 1st ed. John Wiley and Sons, Cambridge (United States).

Elzinga, E.J., 2012. Formation of layered Fe(II)-Al(III)-hydroxides during reaction of Fe (II) with aluminum oxide. Environ. Sci. Technol. 46, 4894–4901. https://doi.org/10.1021/es2044807.

EPA, 2002. Radionuclides in Drinking Water: A Small Entity Compliance Guide. https://www.epa.gov/sites/production/files/2015-06/documents/compliance-radionuclidesindw.pdf.

Forano, C., Costantino, U., Prévot, V., Gueho, C.T., 2013. Layered Double Hydroxides (LDH). https://doi.org/10.1016/B978-0-08-098258-8.00025-0.

Geraedts, K., Maes, A., 2008. Determination of the conditional interaction constant between colloidal technetium(IV) and Gorleben humic substances. Appl. Geochem. 23, 1127–1139. https://doi.org/10.1016/j.apgeochem.2007.11.007.

Goh, K.H., Lim, T.T., Dong, Z., 2008. Application of layered double hydroxides for removal of oxyanions: a review. Water Res. 42, 1343–1368. https://doi.org/10.1016/j.watres.2007.10.043.

Gorski, C.A., Edwards, R., Sander, M., Hofstetter, T.B., Stewart, S.M., 2016. Thermodynamic characterization of Iron oxide–Aqueous Fe^{2+} redox couples. Environ. Sci. Technol. 50, 8538–8547. https://doi.org/10.1021/acs.est.6b02661.

Grambow, B., Gaona, X., Runde, W., Konings, R., Plyasunov, A.V., Rao, L., Smith, A.L., Moore, E., Ragoussi, M.-E., Martinez-Gonzalez, J., Grenthe, I., 2018. Chemical thermodynamics of technetium in the OECD/NEA update volume. Tc&Re ISTR2018 Int. Symp. Technetium Rhenium. pp. 35–49. https://doi.org/10.13140/RG.2.2.31901.36328.

Guillaumont, R., Fanghänel, T., Neck, V., Fuger, J., Palmer, D.A., Grenthe, I., Rand, M.H., 2003. Update on the Chemical Thermodynamics of Uranium, Neptunium, Plutonium, Americium and Technetium. OECD, Issy-les-Moulineaux, France, pp. 4.

Hanesch, M., 2009. Raman spectroscopy of iron oxides and (oxy)hydroxides at low laser power and possible applications in environmental magnetic studies. Geophys. J. Int. 177, 941–948. https://doi.org/10.1111/j.1365-246X.2009.04122.x.

Huo, L., Xie, W., Qian, T., Guan, X., Zhao, D., 2017. Reductive immobilization of pertechnetate in soil and groundwater using synthetic pyrite nanoparticles. Chemosphere 174, 456–465. https://doi.org/10.1016/j.chemosphere.2017.02.018.

Johannsen, B., Spies, H., 1996. Technetium(V) chemistry as relevant to nuclear medicine. Top. Curr. Chem. 176, 77–121. https://doi.org/10.1007/3-540-59469-8_4.

Jolivet, J.P., Tronc, E., Chanéac, C., 2006. Iron oxides: From molecular clusters to solid. A nice example of chemical versatility. C. R. Geosci. 338, 488–497. https://doi.org/10.1016/j.crte.2006.04.014.

Kadarisman, S., Abidin, E.L., Marlina, I.S., Setiawan, H., 2018. Synthesis of nano-α-Al_2O_3 for 99_{Mo} adsorbent. Atom Indones. 44, 17–21. https://doi.org/10.1016/B978-0-444-63587-7/00015-9.

Kergourlay, F., Réguer, S., Neff, D., Foy, E., Picca, F.E., Saheb, M., Hustache, S., Mirambet, F., Dillmann, P., 2018. Stabilization treatment of cultural heritage artefacts: in situ monitoring of marine iron objects dechlorinated in alkali solution. Corros. Sci. 132, 21–34. https://doi.org/10.1016/j.corsci.2017.12.028.

Kimura, Y., Sato, T., Nakamura, N., Nozawa, J., Nakamura, T., Tsukamoto, K., Yamamoto, K., 2013. Vortex magnetic structure in framboidal magnetite reveals existence of water droplets in an ancient asteroid. Nat. Commun. 4, 1–8. https://doi.org/10.1038/ncomms3649.

Kobayashi, T., Scheinost, A.C., Fellhauer, D., Gaona, X., Altmaier, M., 2013. Redox behavior of Tc(VII)/Tc(IV) under various reducing conditions in 0.1 M NaCl solutions.

Radiochim. Acta 101, 323–332. https://doi.org/10.1524/ract.2013.2040.
Kumar, S., Rawat, N., Kar, A.S., Tomar, B.S., Manchanda, V.K., 2011. Effect of humic acid on sorption of technetium by alumina. J. Hazard. Mater. 192, 1040–1045. https://doi.org/10.1016/j.jhazmat.2011.06.007.
Lemire, R.J., Berner, U., Musikas, C., Palmer, D.A., Taylor, P., Tochiyama, O., 2013. Chemical Thermodynamics of Iron. Part 1, OECD Nucle. OECD, Paris, France.
Levitskaia, T.G., Chatterjee, S., Pence, N.K., Romero, J., Varga, T., Engelhard, M.H., Du, Y., Kovarik, L., Arey, B.W., Bowden, M.E., Walter, E.D., 2016. Inorganic tin aluminophosphate nanocomposite for reductive separation of pertechnetate. Environ. Sci. Nano 3, 1003–1013. https://doi.org/10.1039/c6en00130k.
Li, F.B., Tao, L., Feng, C.H., Li, X.Z., Sun, A.W., 2009. Electrochemical evidences for promoted interfacial reactions: the role of Fe(II) adsorbed onto γ-Al_2O_3 and TiO_2 in reductive transformation of 2-nitrophenol. Environ. Sci. Technol. 43, 3656–3661. https://doi.org/10.1021/es8033445.
Lieser, K.H., Bauscher, C., 1987. Technetium in the hydrosphere and in the geosphere. I chemistry of technetium and iron in natural waters and influence of the redox potential on the sorption of technetium. Radiochim. Acta 42, 205–213.
Liu, Y., Terry, J., Jurisson, S., 2008. Pertechnetate immobilization with amorphous iron sulfide. Radiochim. Acta 96, 823–833. https://doi.org/10.1524/ract.2008.1528.
Liu, Y., Wang, X., Chen, J., Fu, D., Pang, H., Wu, Y., Yu, S., Wang, X., 2018. Environmental remediation of heavy metal ions by novel-nanomaterials: a review. Environ. Pollut. 246, 608–620. https://doi.org/10.1016/j.envpol.2018.12.076.
Luksic, S.A., Kim, D., Um, W., Wang, G., Schweiger, M.J., Soderquist, C.Z., Lukens, W., Kruger, A.A., 2018. Effect of Technetium-99 sources on its retention in low activity waste glass. J. Nucl. Mater. 503, 235–244. https://doi.org/10.1016/j.jnucmat.2018.02.019.
Lutz, H.D., Möller, H., Schmidt, M., 1994. Molecular structure Lattice vibration spectra. Part LXXXII. Brucite-type hydroxides $M(OH)_2$ (M = Ca, Mn, Co, Fe, Cd) - IR and Raman spectra, neutron diffraction of $Fe(OH)_2$. J. Mol. Struct. 328, 121–132. https://doi.org/10.1039/c3an01507f.
Ma, B., Charlet, L., Fernandez-Martinez, A., Kang, M., Madé, B., 2019. A review of the retention mechanisms of redox-sensitive radionuclides in multi-barrier systems. Appl. Geochem. 100, 414–431. https://doi.org/10.1016/j.apgeochem.2018.12.001.
Marlina, M., Sarmini, E., Herlina, S., Saptiama, I., Setiawan, H., Kadarisman, K., 2017. Preparation and characterization of zirconia nanomaterial as a Molybdenum-99 adsorbent. Atom Indones. 43, 1–6. https://doi.org/10.17146/aij.2017.587.
Marshall, T.A., Morris, K., Law, G.T.W., Mosselmans, J.F.W., Bots, P., Parry, S.A., Shaw, S., 2014. Incorporation and retention of 99-Tc(IV) in magnetite under high pH conditions. Environ. Sci. Technol. 48, 11853–11862. https://doi.org/10.1021/es503438e.
Mayordomo, N., Foerstendorf, H., Lützenkirchen, J., Heim, K., Weiss, S., Alonso, Ú., Missana, T., Schmeide, K., Jordan, N., 2018. Selenium(IV) sorption onto γ-Al_2O_3: a consistent description of the surface speciation by spectroscopy and thermodynamic modeling. Environ. Sci. Technol. 581–588. https://doi.org/10.1021/acs.est.7b04546.
Mayordomo, N., Alonso, U., Missana, T., 2019. Effects of γ-alumina nanoparticles on strontium sorption in smectite: additive model approach. Appl. Geochem. 100, 121–130. https://doi.org/10.1016/j.apgeochem.2018.11.012.
Meena, A.H., Arai, Y., 2017. Environmental geochemistry of technetium. Environ. Chem. Lett. 15, 241–263. https://doi.org/10.1007/s10311-017-0605-7.
Meyer, R.E., Arnold, W.D., Case, F.I., O´Kelley, G.D.O., 1991. Solubilities of Tc(IV) oxides. Radiochim. Acta 55, 11–18.
Missana, T., Benedicto, A., Mayordomo, N., Alonso, U., 2014. Analysis of anion adsorption effects on alumina nanoparticles stability. Appl. Geochem. 49, 68–76. https://doi.org/10.1016/j.apgeochem.2014.04.003.
Moreno Gil, N., Badillo Almaraz, V.E., Olivé, K.I., 2019. Evaluation of TiO_2 nanomaterials as potential sorbents for $^{99}Mo/^{99m}Tc$ generator. AIP Conf. Proc. 2090. https://doi.org/10.1063/1.5095900. 030005-1–4.
Nano, G.V., Strathmann, T.J., 2006. Ferrous iron sorption by hydrous metal oxides. J. Colloid Interface Sci. 297, 443–454. https://doi.org/10.1016/j.jcis.2005.11.030.
Pepper, S.E., Bunker, D.J., Bryan, N.D., Livens, F.R., Charnock, J.M., Pattrick, R.A.D., Collison, D., 2003. Treatment of radioactive wastes: an X-ray absorption spectroscopy study of the reaction of technetium with green rust. J. Colloid Interface Sci. 268, 408–412. https://doi.org/10.1016/j.jcis.2003.08.024.
Peretyazhko, T., Zachara, J.M., Heald, S.M., Jeon, B.H., Kukkadapu, R.K., Liu, C., Moore, D., Resch, C.T., 2008a. Heterogeneous reduction of Tc(VII) by Fe(II) at the solid-water interface. Geochim. Cosmochim. Acta 72, 1521–1539. https://doi.org/10.1016/j.gca.2008.01.004.
Peretyazhko, T., Zachara, J.M., Heald, S.M., Kukkadapu, R.K., Liu, C., Plymale, A.E., Resch, C.T., 2008b. Reduction of Tc(VII) by Fe (II) sorbed on Al(hydr)oxides. Environ. Sci. Technol. 42, 5499–5506.
Poineau, F., Fattahi, M., Grambow, B., 2006. Condensation mechanisms of tetravalen technetium in chloride media. Radiochim. Acta 94, 291–299.
Rozov, K., Berner, U., Taviot-Gueho, C., Leroux, F., Renaudin, G., Kulik, D., Diamond, L.W., 2010. Synthesis and characterization of the LDH hydrotalcite-pyroaurite solid-solution series. Cem. Concr. Res. 40, 1248–1254. https://doi.org/10.1016/j.cemconres.2009.08.031.
Saslow, S.A., Um, W., Pearce, C.I., Bowden, M.E., Engelhard, M.H., Lukens, W.L., Kim, D.S., Schweiger, M.J., Kruger, A.A., 2018. Cr(VI) effect on Tc-99 removal from Hanford Low-Activity waste simulant by ferrous hydroxide. Environ. Sci. Technol. 52, 11752–11759. https://doi.org/10.1021/acs.est.8b03314.
Saslow, S.A., Um, W., Pearce, C.I., Engelhard, M.H., Bowden, M.E., Lukens, W., Leavy, I.I., Riley, B.J., Kim, D.-S., Schweiger, M.J., Kruger, A.A., 2017. Reduction and simultaneous removal of ^{99}Tc and Cr by $Fe(OH)_2$ (s) mineral transformation. Environ. Sci. Technol. 51, 8635–8642. https://doi.org/10.1021/acs.est.7b02278.
Sellin, P., Leupin, O.X., 2014. The use of clay as an engineered barrier in radioactive-waste management - A review. Clays Clay Miner. 61, 477–498. https://doi.org/10.1346/CCMN.2013.0610601.
Stookey, L.L., 1970. Ferrozine-a new spectrophotometric reagent for Iron. Anal. Chem. 42, 779–781. https://doi.org/10.1021/ac60289a016.
Um, W., CHang, H., Icenhower, J.P., Lukens, W.W., Serne, R.J., Qafoku, N.P., Westsik Jr., J.H., Buck, E.C., Smith, S.C., 2011. Immobilization and limited reoxidation of Technetium-99 by Fe(II) -Goethite and limited reoxidation. Environ. Sci. Technol. 45, 4904–4913.
Usman, M., Byrne, J.M., Chaudhary, A., Orsetti, S., Hanna, K., Ruby, C., Kappler, A., Haderlein, S.B., 2018. Magnetite and green rust: synthesis, properties, and environmental applications of mixed-valent iron minerals. Chem. Rev. 118, 3251–3304. https://doi.org/10.1021/acs.chemrev.7b00224.
van der Lee, J., de Wint, L., 1999. Chess Tutorial and Cookbook, Technical Repot LHM/RD/99/05.
Wang, Q., Gao, Y., Luo, J., Zhong, Z., Borgna, A., Guo, Z., O'Hare, D., 2013. Synthesis of nano-sized spherical Mg_3Al–CO_3 layered double hydroxide as a high-temperature CO_2 adsorbent. RSC Adv. 3, 3414. https://doi.org/10.1039/c2ra22607c.
Weaver, J., Soderquist, C.Z., Washton, N.M., Lipton, A.S., Gassman, P.L., Lukens, W.W., Kruger, A.A., Wall, N.A., McCloy, J.S., 2017. Chemical trends in solid alkali pertechnetates. Inorg. Chem. 56, 2533–2544. https://doi.org/10.1021/acs.inorgchem.6b02694.
Wester, D.W., White, D.H., Miller, F.W., Dean, R.T., Schreifels, J.A., Hunt, J.E., 1987. Synthesis and characterization of technetium complexes with phosphoruscontaining ligands. The homoleptic trimethylphosphite, dimethylmethylphosphonite and methyldiethylphosphinite technetium(I) cations. Inorganica Chim. Acta 131, 163–169. https://doi.org/10.1016/S0020-1693(00)96019-5.
Yalçıntaş, E., Scheinost, A.C., Gaona, X., Altmaier, M., 2016. Systematic XAS study on the reduction and uptake of Tc by magnetite and mackinawite. Dalton Trans. 19, 17874–17885. https://doi.org/10.1039/C6DT02872A.
Zachara, J.M., Heald, S.M., Jeon, B.-H., Kukkadapu, R.K., Liu, C., 2007. Reduction of pertechnetate [Tc(VII)] by aqueous Fe(II) and the nature of solid phase redox products. Geochim. Cosmochim. Acta 71, 2137–2157. https://doi.org/10.1016/j.gca.2006.10.025.
Zhu, Z., Tao, L., Li, F., 2013. Effects of dissolved organic matter on adsorbed Fe(II) reactivity for the reduction of 2-nitrophenol in TiO_2 suspensions. Chemosphere 93, 29–34. https://doi.org/10.1016/j.chemosphere.2013.04.053.

Supplementary material

Technetium retention by gamma alumina nanoparticles and the effect of sorbed Fe^{2+}

Natalia Mayordomo[1]*, Diana M. Rodríguez[1], Dieter Schild[2], Konrad Molodtsov[1], Erik V. Johnstone[3], René Hübner[4], Salim Shams Aldin Azzam,[1] Vinzenz Brendler[1] and Katharina Müller[1]*.

[1]Helmholtz-Zentrum Dresden-Rossendorf (HZDR). Institute of Resource Ecology, Bautzner Landstrasse 400, 01328, Dresden (Germany).

[2]Karlsruhe Institute of Technology (KIT). Institute for Nuclear Waste Disposal (INE), Hermann-von-Helmholtz-Platz 1, 76344 Eggenstein-Leopoldshafen, (Germany).

[3]Innovative Fuel Solutions (IFS), 89031, North Las Vegas, NV (USA).

[4]Helmholtz-Zentrum Dresden-Rossendorf (HZDR). Institute of Ion Beam Physics and Materials Research, Bautzner Landstrasse 400, 01328, Dresden (Germany).

Corresponding authors: *n.mayordomo-herranz@hzdr.de, *k.mueller@hzdr.de

Keywords: Technetium, Al_2O_3, reduction, sorption, immobilization

S1. Synthesis of the Fe(II)-Al(III)-Cl layered double hydroxide (LDH).

The synthesis of the Fe(II)-Al(III)-Cl layered double hydroxide (LDH) was carried out in a glove box with O_2 concentration < 2 ppm. The procedure was similar to the one reported by Zhong *et al.* [1]. The synthesis consisted of the co-precipitation of the Fe(II)-Al(III)-Cl LDH when 0.02 mol of $AlCl_3 \cdot 6H_2O$ (> 99% Alfa Aesar) slowly dissolved in 200 mL of degassed deionized water were mixed with 0.03 mol of $FeCl_2 \cdot 4H_2O$ (> 99%, Aldrich) in 200 mL of water. The resulting solution was set at pH 9.5 by addition of 200 mL of a 2 M NaOH solution. The co-precipitation of the Fe(II)-Al(III)-Cl LDH was immediately observed with increasing the pH. Then, the suspension was heated up to 65 °C and ultrasound was applied for 30 minutes by using an ultrasound finger. The resulting suspension was washed with degassed water and then centrifuged at 600 g for 30 min, after which, the supernatant was removed. The latter process was repeated thrice.

The synthetic Fe(II)-Al(III)-Cl LDH was finally dried with a lyophilizator (Christ alpha 1-4) and homogenized with an agate mortar inside the glove box. The diffractogram of the synthetic solid is shown in the Figure S1. The diffractogram coincide with the ones already reported for Fe(II)-Al(III) LDH phases [1,2].

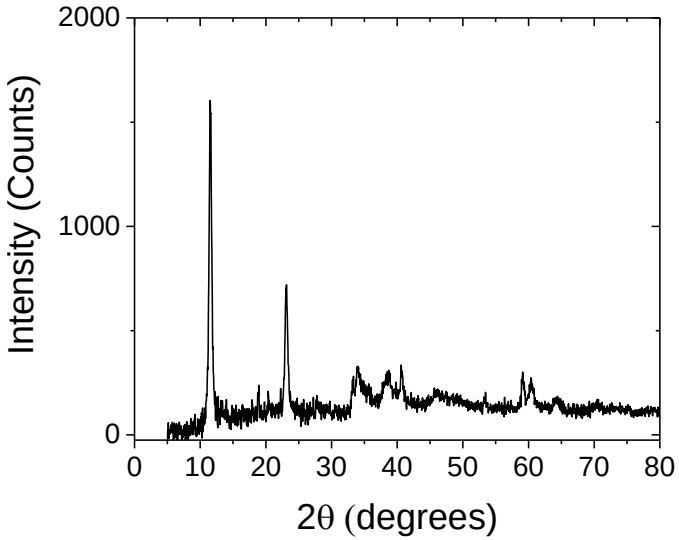

Figure S1. X-ray powder diffractogram of the synthetic Fe(II)-Al(III)-Cl layered double hydroxide.

S2. Detailed experimental set up for batch contact experiments.

For the batch contact experiments in the ternary system, we have followed a similar procedure than the one carried out by Peretyazhko *et al.* [3]. However, we have used lower amounts of the sorbent and $FeCl_2$: down to 0.5 $g \cdot L^{-1}$ γ-Al_2O_3 (instead of 3 $g \cdot L^{-1}$) and 60 µM $FeCl_2$ (instead of 0.1 mM Fe^{2+}). The amount of Tc(VII) used was 5 µM in order to keep the same ratio Fe(II)/Tc(VII) = 12 as used in [3]. The reduced $FeCl_2$ concentration was used to ensure the heterogeneous Tc(VII) reduction.

One set of experiments consisted of evaluating the effect of pH (from pH 4 to pH 10) and ionic strength (H_2O and 0.25 M NaCl) on the Tc retention. Suspensions were sampled after 7 and 30 days of contact. The other set of experiments evaluated the kinetics of Tc retention on the ternary system (from 30 minutes to 30 days) under different pH values (4.8, 7.0 and 9.5).

60 µM $FeCl_2$ aqueous solutions were prepared by addition of 2 mM $FeCl_2$ stock solution in 50 mL of water in Eppendorf tubes®, then pH was adjusted. After two days of equilibration, 10 mL of solution were extracted as *blank solution* and the remaining 40 mL were used for the *ternary system experiments*.

The *ternary system experiments* were carried out by adding γ-Al_2O_3 powder to 60 µM $FeCl_2$ solution and, after 2 days of equilibration, Tc(VII) was added in the suspension. The suspensions were kept under continuous horizontal stirring. Kinetically, 2 x 2.5 mL of suspension were sampled. The first was directly centrifuged at 600 g for 1 hour, and then two 0.25 mL aliquots were taken for determining the Tc and Fe^{2+} concentration in solution by LSC and UV-vis, respectively. Furthermore, the pH and Eh of supernatant were measured. The second was acidified with 0.25 mL of 6 M HCl with the aim of re-dissolving the Fe^{2+} that is sorbed on the γ-Al_2O_3 or taking part of soluble Fe(II) solids. After 1h under acidic conditions, the suspension is centrifuged at 600 g for 1 hour and a 0.25 mL aliquot of supernatant is taken to evaluate the Fe^{2+} concentration after re-dissolution.

The *blank solution* was sampled at the same time as the ternary system. In this case, 2 x 0.25 mL of solution were taken. The first was taken to evaluate the amount of Fe^{2+} in solution by UV-vis. The second was acidified with 0.25 mL of 6 M HCl for one hour and then centrifuged at 600 g for 1 hour. Afterwards, 0.25 mL of the supernatant were taken to evaluate the amount of Fe^{2+} after re-dissolution by UV-vis. The measured Fe^{2+} concentration in solution and after re-dissolution had negligible differences; therefore, the Fe^{2+} shown in the graphs was calculated as an average of both.

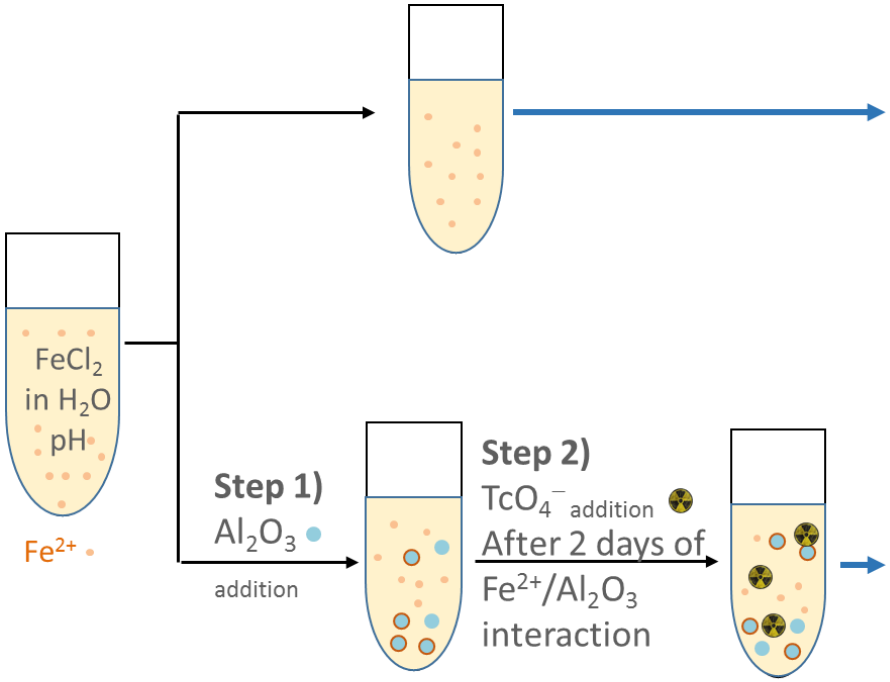

Blank solution
Kinetic monitoring
- pH and Eh
- $[Fe^{2+}]$ as average of :
  1. $[Fe^{2+}]_{solution}$
  2. $[Fe^{2+}]_{after\ re\text{-}dissolution}$

Ternary system
Kinetically monitoring
- pH and Eh
- $[Tc]_{solution}$
- $[Fe^{2+}]_{solution}$
- $[Fe^{2+}]_{after\ re\text{-}dissolution}$

Conditions and materials
N_2 atmosphere (O_2 and CO_2 free)
$[Fe^{2+}] = 6 \cdot 10^{-5}$ M
$[Al_2O_3] = 0.5\ g \cdot L^{-1}$
$[TcO_4^-] = 5 \cdot 10^{-6}$ M

Methods
- **$[Fe^{2+}]_{solution,\ after\ re\text{-}dissolution}$**

→ **UV-vis ; ferrozine assay**, i.e. 0.25 mL of sample in 2 mL of 1 g · L^{-1} ferrozine (50mM HEPES, pH 7)
At 562 nm and ε = 279000 $(Mcm)^{-1}$
- **$[Tc]_{solution}$**

→ **Liquid Scintillation Counter (LSC)**
0.25 mL of sample in 5 mL of scintilliator liquid

- **$[Fe^{2+}]_{solution}$ and $[Tc]_{solution}$**

i. Centrifugation of 2.5 mL suspension 600 g for 1h
ii. Supernatant analysis
  1. $[Fe^{2+}]_{solution}$ → Ferrozine essay
  1. $[Tc]_{solution}$ → LSC

- **$[Fe^{2+}]_{after\ re\text{-}dissolution}$**

i. Addition of 0.250 mL 6 M HCl to 2.5 mL suspension (1h contact)
ii. Centrifugation 600 g for 1h
iii. Supernatant analysis
  1. $[Fe^{2+}]_{after\ re\text{-}dissolution}$ → Ferrozine essay

Figure S2. Scheme of sampling and experimental set up of batch experiments for analyzing Tc retention on γ-Al_2O_3 in presence of sorbed Fe^{2+}.

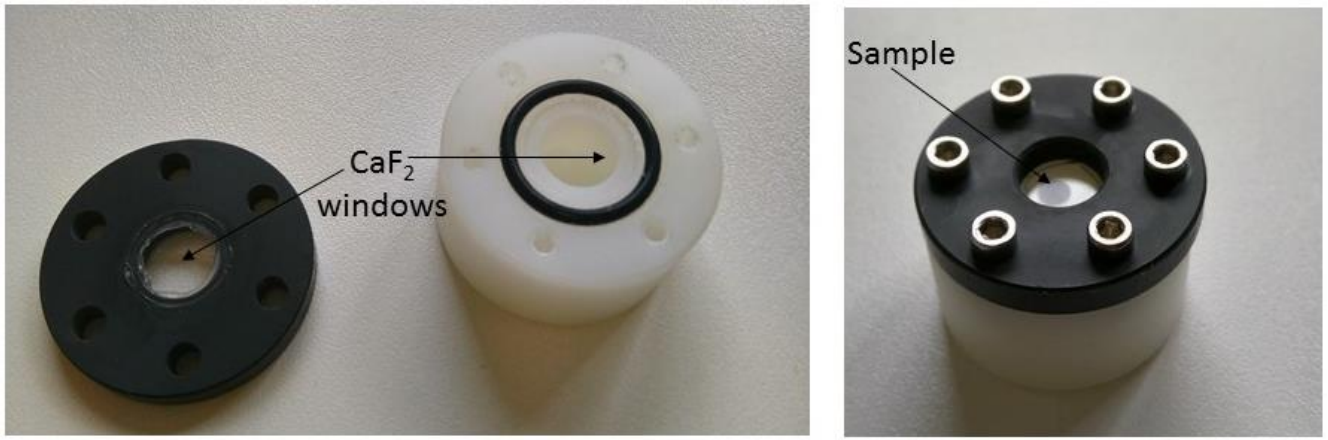

Figure S3. Cell used in Raman microscopic measurements (left) disassembled and (right) assembled containing a sample.

The cell consists of a PVC lid containing a glued 0.5 mm thick CaF_2 window and a base made of polyoxymethylene with a 1 cm deep hole, created to avoid the peaks coming from the polyoxymethylene, over which lies another 0.5 mm thick CaF_2 window and a surrounding rubber o-ring. Both parts are screwed inside the glove box. This assembly ensures the absence of O_2 inside the cell.

S3. Detailed experimental set up for X-ray diffraction (XRD) measurements.

Several XRD measurements were carried out with the aim of identifying the secondary phases formed in the experiments. The precipitates resulting of the following samples were measured: (1) 60 µM Fe^{2+} at pH 9.5, 0.5 $g \cdot L^{-1}$ γ–Al_2O_3 in contact with 60 µM Fe^{2+}at (2) pH 7.5 and (3) pH 9.5 and 0.5 $g \cdot L^{-1}$ γ–Al_2O_3 containing pre-sorbed Fe^{2+} in contact with 5 µM $Tc(VII)O_4^-$ at (4) pH 4.5, (5) pH 7 and (6) pH 9.5.

The sample preparation took place inside the N_2 glove box (O_2 < 0.5 ppm). After the samples were in constant horizontal stirring for seven days, they were centrifuged at 600 g for 1 h and the supernatant was removed. The solid was dried and then homogenized with an agate mortar. Finally, the solid was deposited on an air-tight sample holder (Rigaku) to ensure N_2 atmosphere while the measurements were performed.

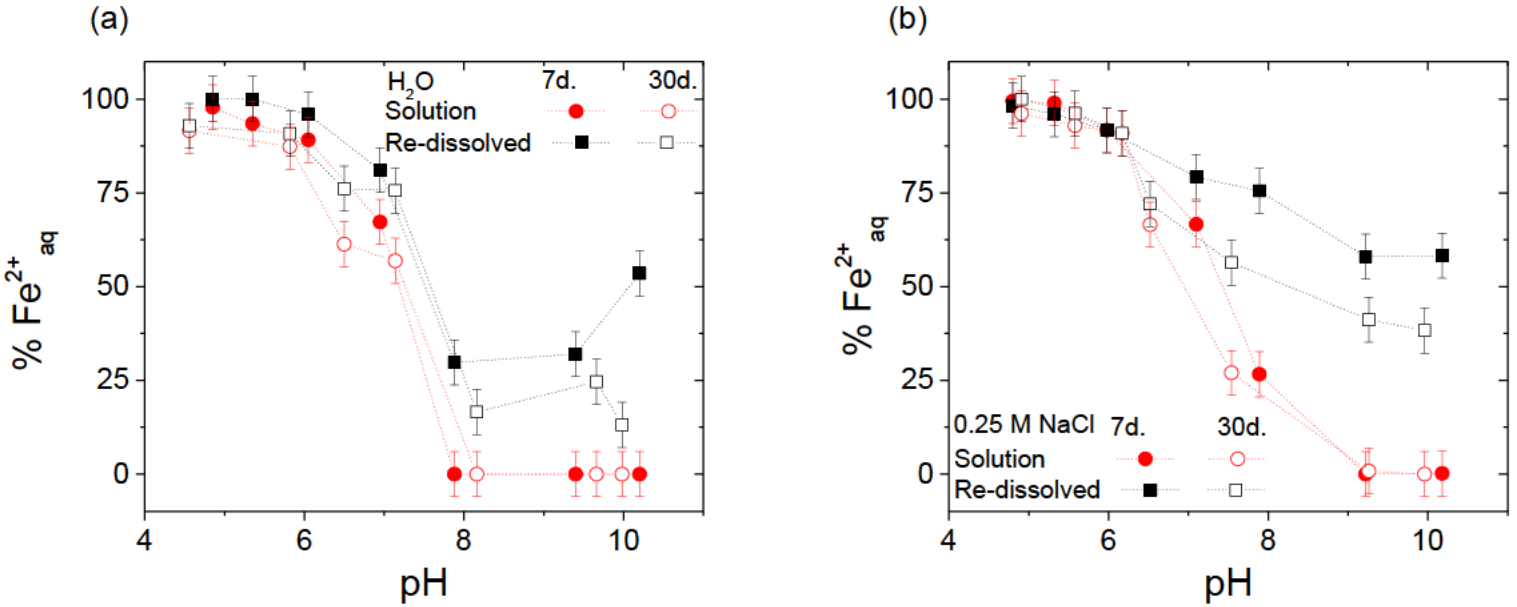

68

69 **Figure S4.** Fe^{2+} aq measured (represented as %) as a function of pH (●,○) directly in solution and (■,□) after acidification of an aliquot, representing the Fe^{2+}fraction
70 after re-dissolution (●,■) 7 days and (○,□) 30 days of contact. The plotted data correspond to the batch experiments to analyze the removed Tc from solution after
71 being in contact with γ-Al_2O_3 containing sorbed Fe^{2+} in (a) H_2O and (b) 0.25 M NaCl (Figure 2).

72

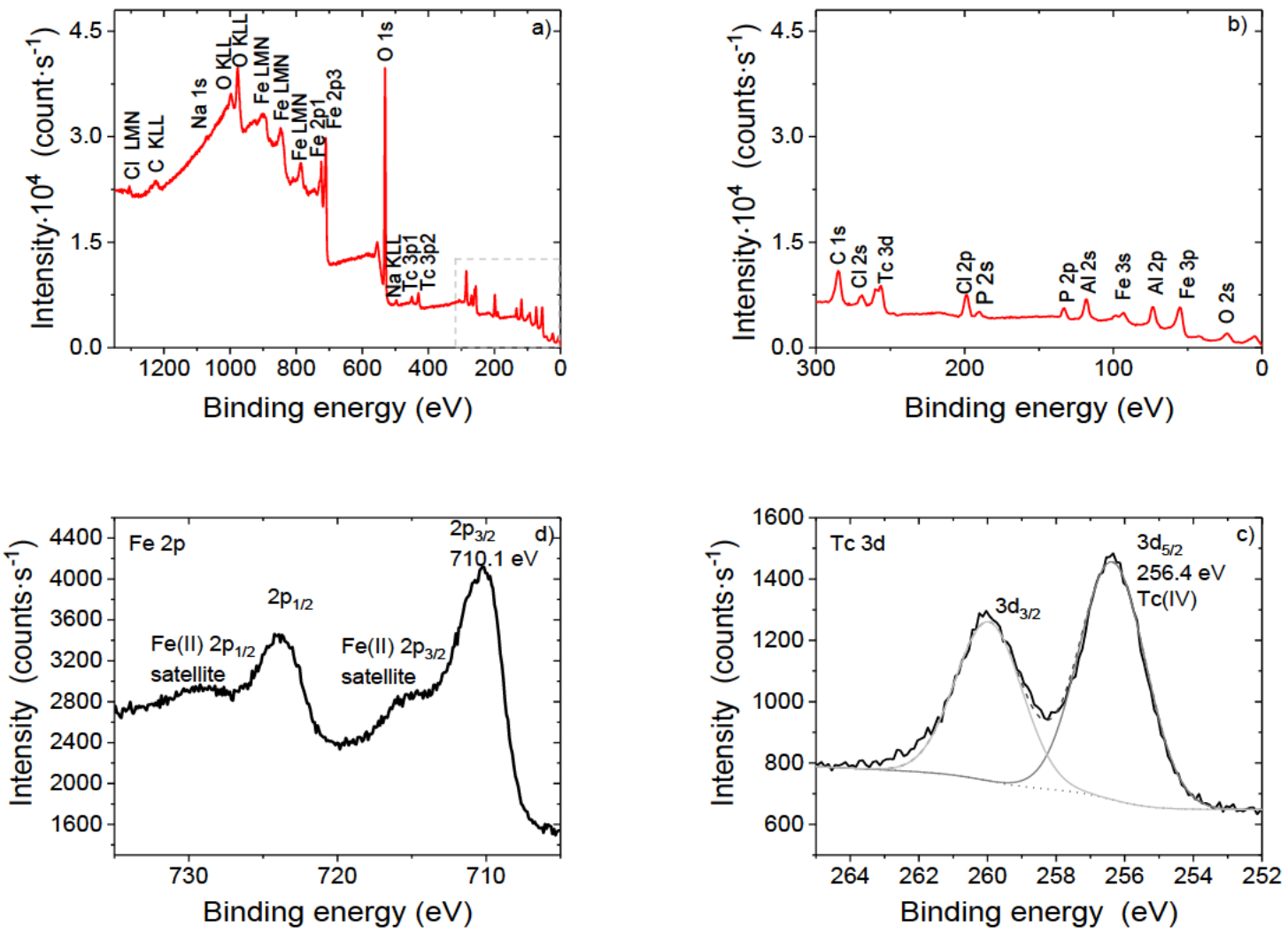

Figure S5. X-ray photoelectron spectra obtained of a dried suspension of γ-Al_2O_3 with sorbed Fe^{2+} after Tc(VII) contact at pH 9.5. (a) full XP spectrum (b) zoomed XP spectrum (c) Fe 2p spectrum and (d) Tc 3d spectrum. $[Tc(VII)]_0$ = 0.5 mM, $[Fe^{2+}]_0$ = 5 mM and 0.5 g·L^{-1} γ-Al_2O_3. Solid lines are the fits of the Tc 3d doublet.

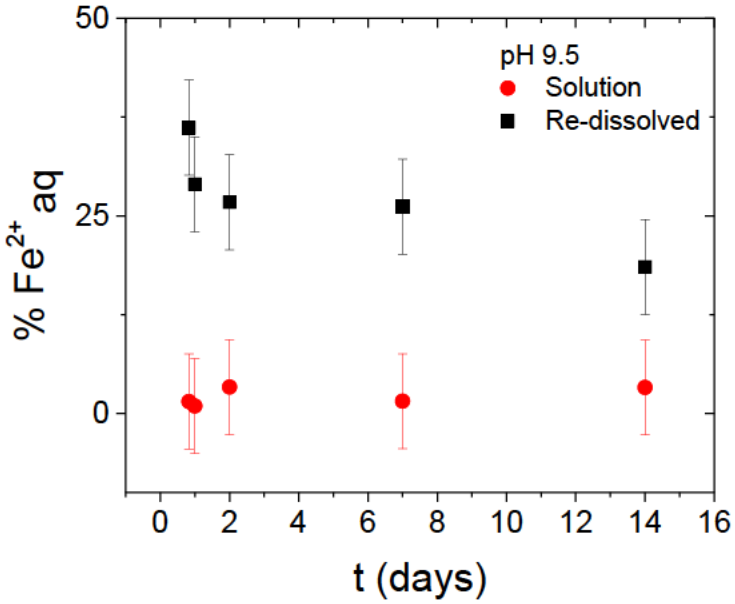

Figure S6. Fe^{2+} aq measured (represented as %) as a function of time (●) directly in solution and (■) after acidification of an aliquot, representing the Fe^{2+}fraction after re-dissolution in a sorption experiment of 60 µM Fe^{2+} on 0.5 $g \cdot L^{-1}$ γ–Al_2O_3 at pH 9.5 in H_2O.

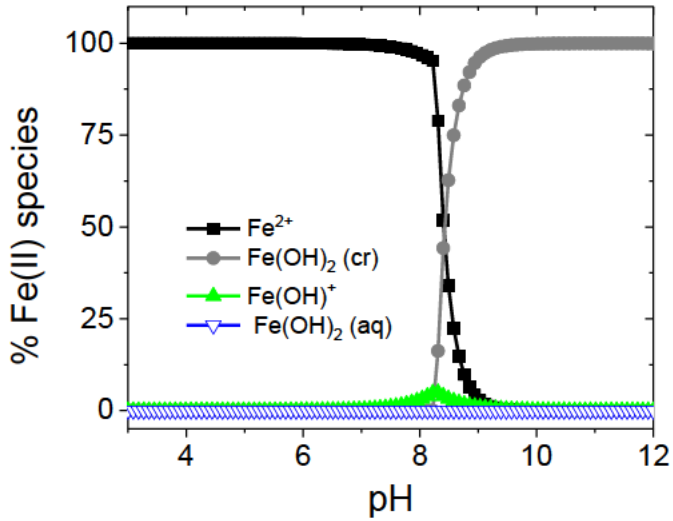

Figure S7. Fe(II) speciation calculated for $[FeCl_2]_0$ = 60 µM in H_2O. The last iron thermodynamic database [4], including the formation constant of $Fe(OH)_2$ [5] were considered for the modeling.

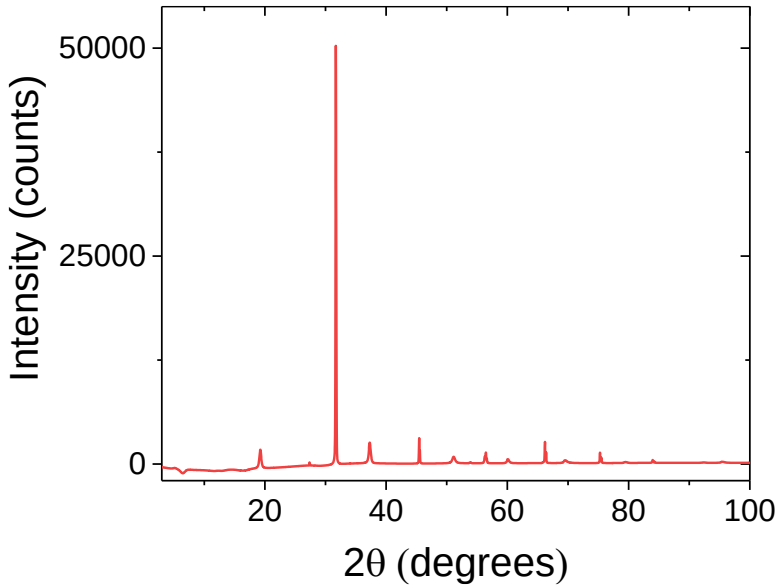

Figure S8. X-ray powder diffractogram of the precipitate resulting from a Fe^{2+} solution at pH 9.5.

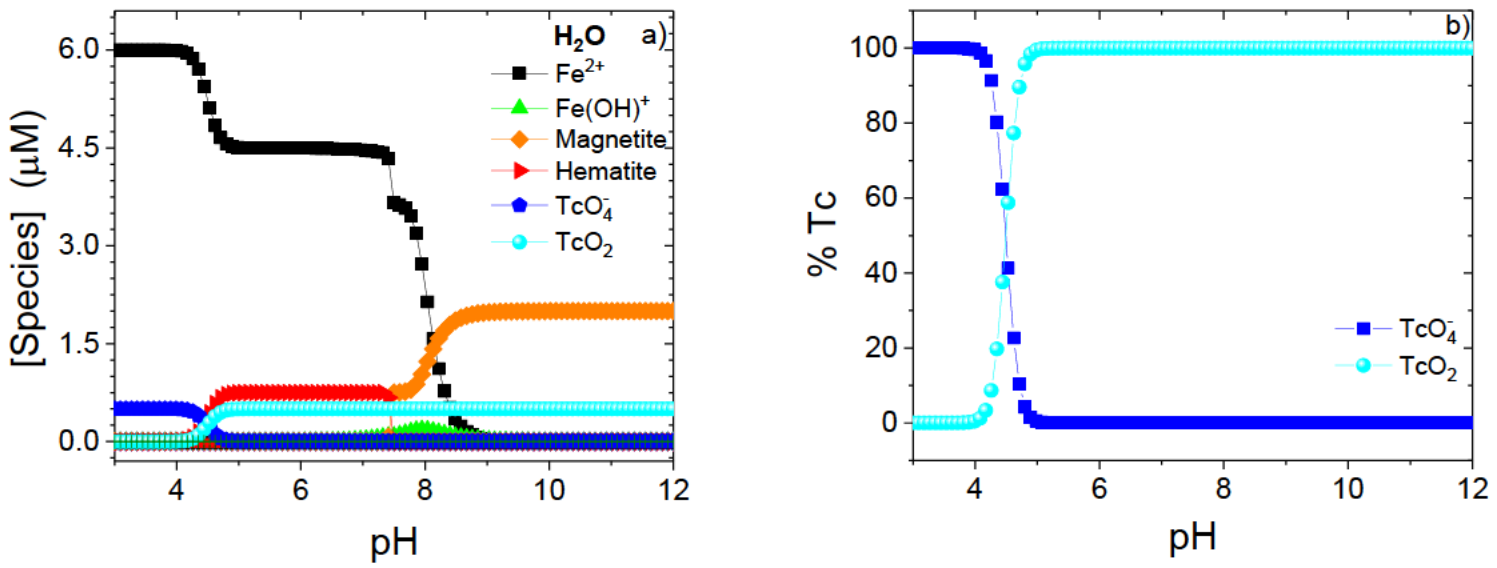

Figure S9. (a) Theoretical concentration of Tc and Fe species as a function of pH when considering $[Tc(VII)]_0 = 5$ μM, $[Fe^{2+}]_0 = 60$ μM. (b) Predicted Tc speciation in (a), represented in percentage. The last iron thermodynamic database [4], including the formation constant of $Fe(OH)_2$ [5] and the latest technetium thermodynamic database [6] were considered for the modeling.

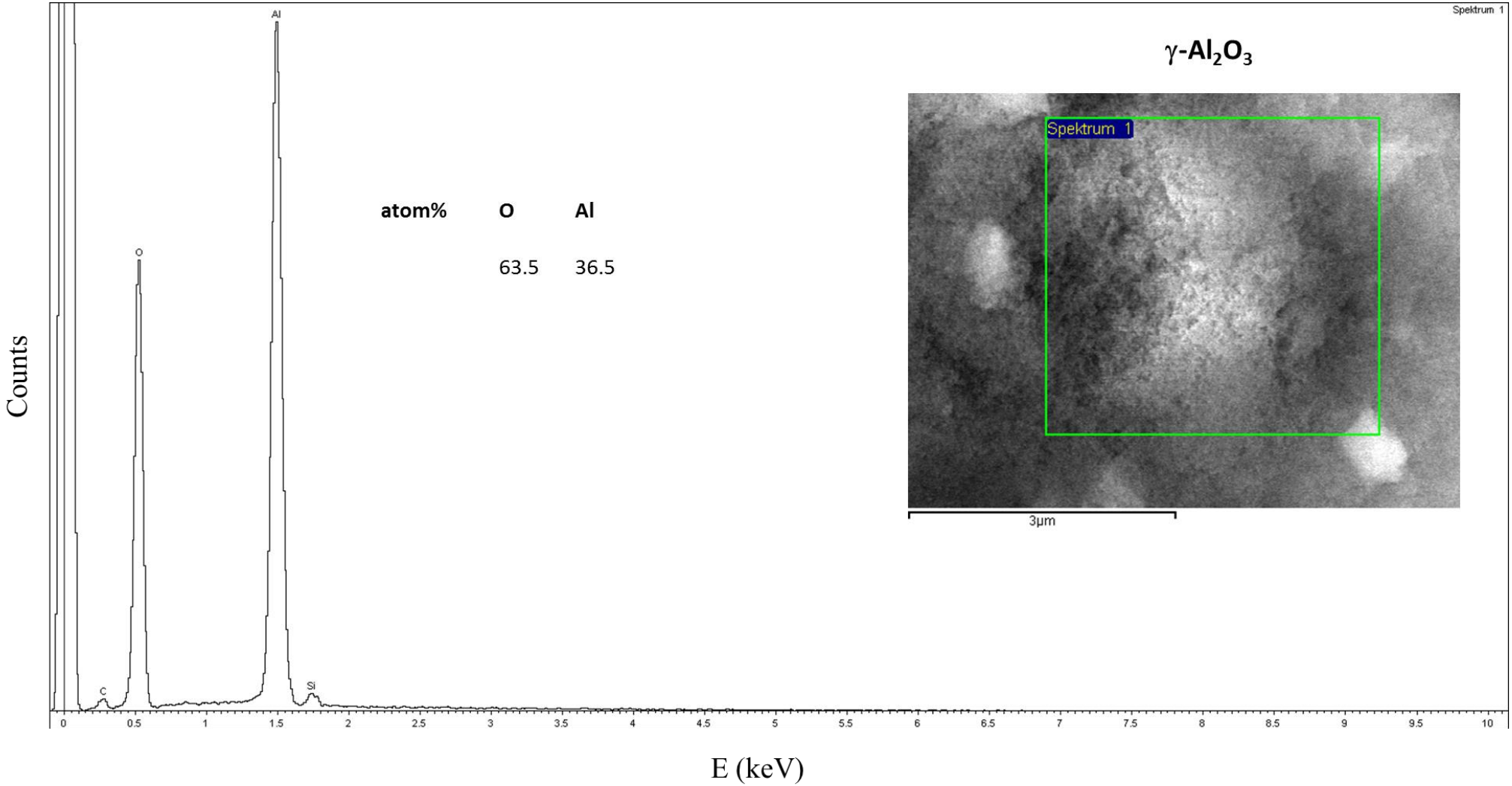

96

97 **Figure S10.** Scanning electron micrograph of and energy dispersive X-ray spectrum of γ-Al_2O_3 at pH 9.0.

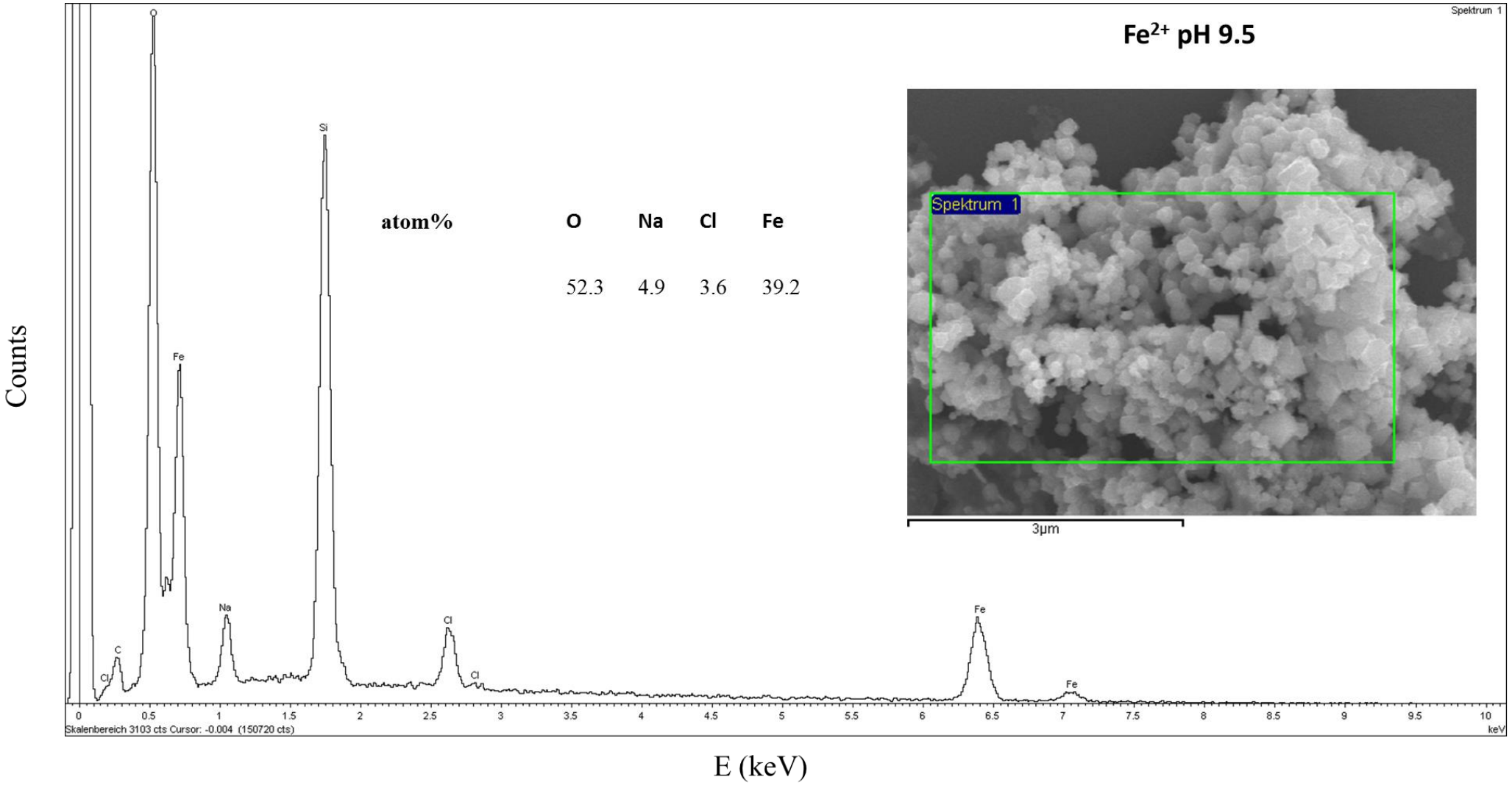

Figure S11. Scanning electron micrograph of and energy dispersive X-ray spectrum of $FeCl_2$ at pH 9.0.

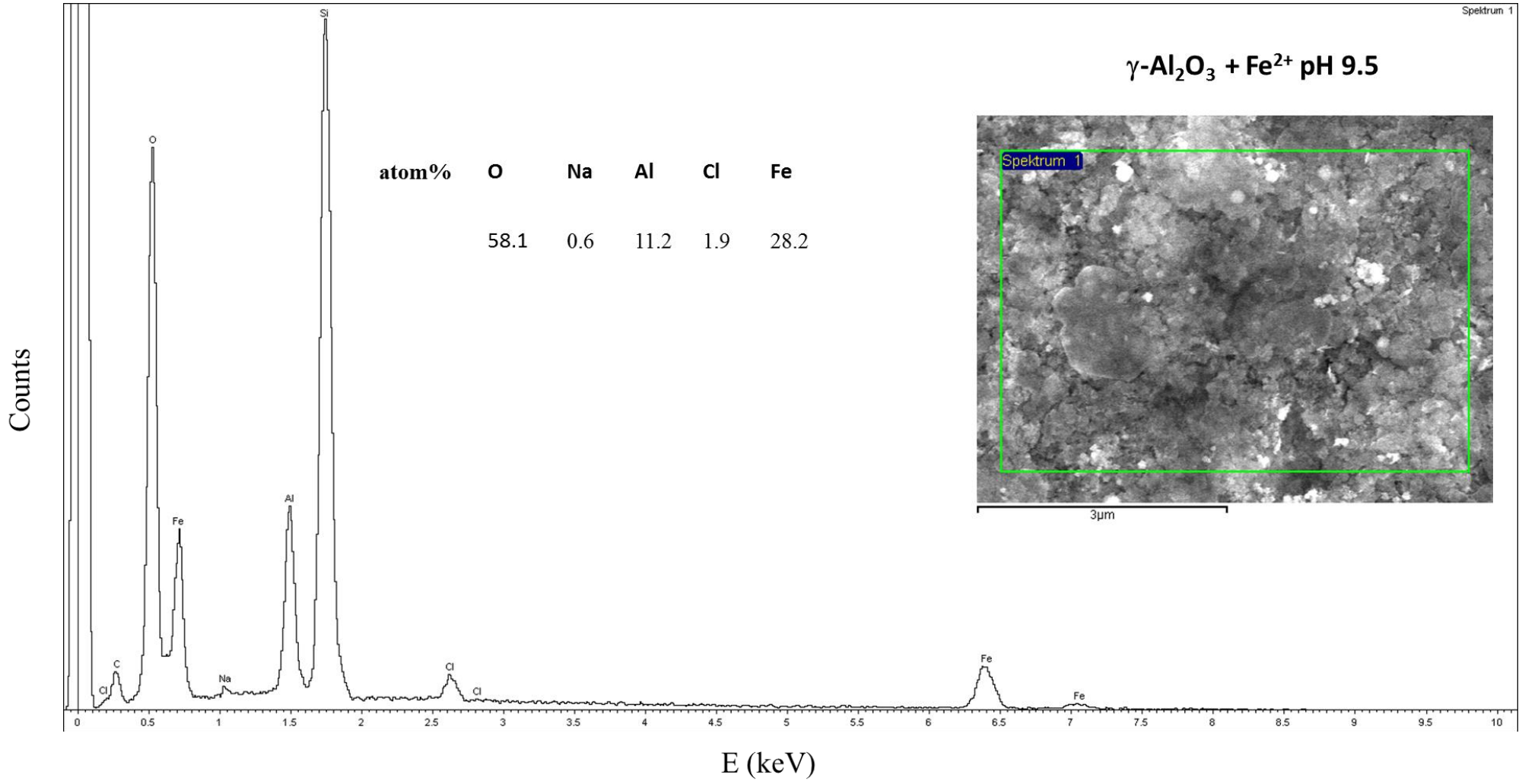

100

101 **Figure S12.** Scanning electron micrograph of and energy dispersive X-ray spectrum of γ-Al_2O_3 with sorbed Fe^{2+} at pH 9.5.

% atom	O-K	Na-K	Al-K	Cl-K	Fe-K	Tc-L
Spot1	57.7		13.0	1.4	26.8	1.1
Spot2	57.2	0.6	12.2	1.9	26.5	1.6
Spot3	62.7	0.3	18.4	1.3	16.5	0.8

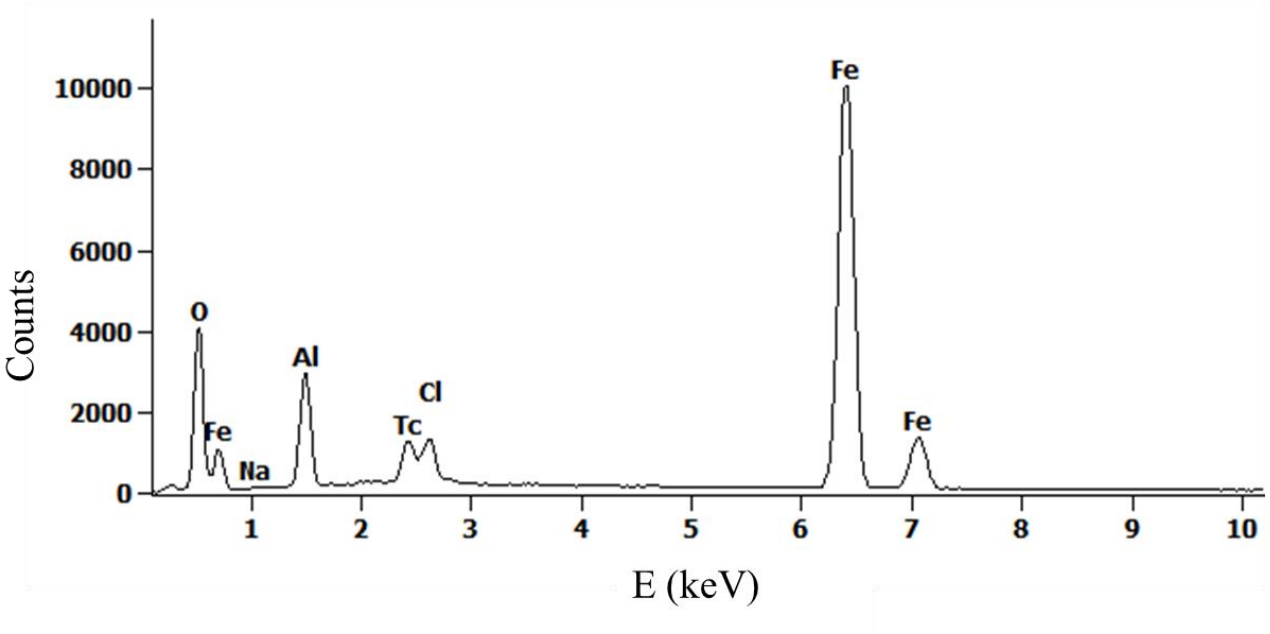

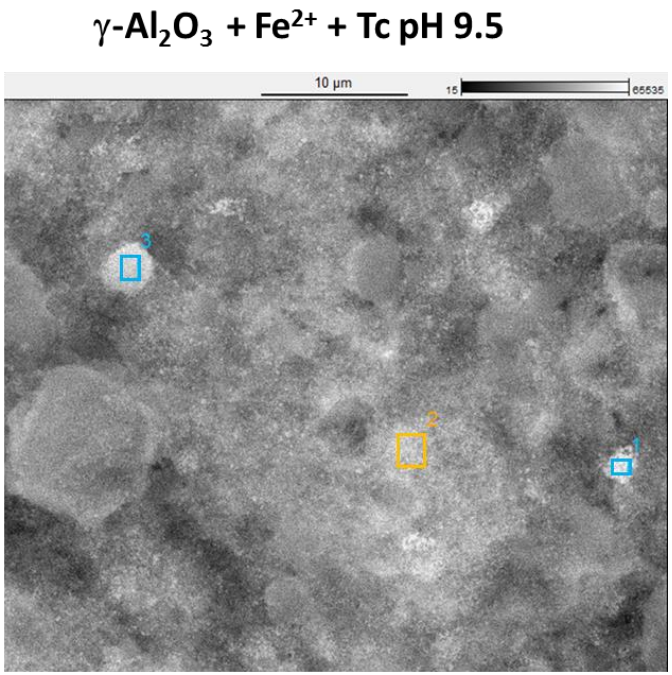

Figure S13. Scanning electron micrograph of and energy dispersive X-ray spectrum γ-Al_2O_3 with sorbed Fe^{2+} after Tc(VII) contact at pH 9.5.

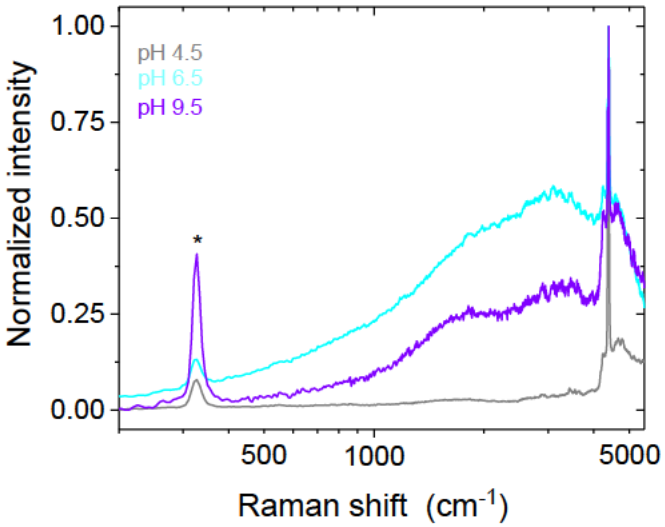

104

105 **Figure S14**. Raman spectra obtained in dried suspensions of γ-Al_2O_3 with sorbed Tc(VII) at various pH. The band (*) corresponds to CaF_2.

106

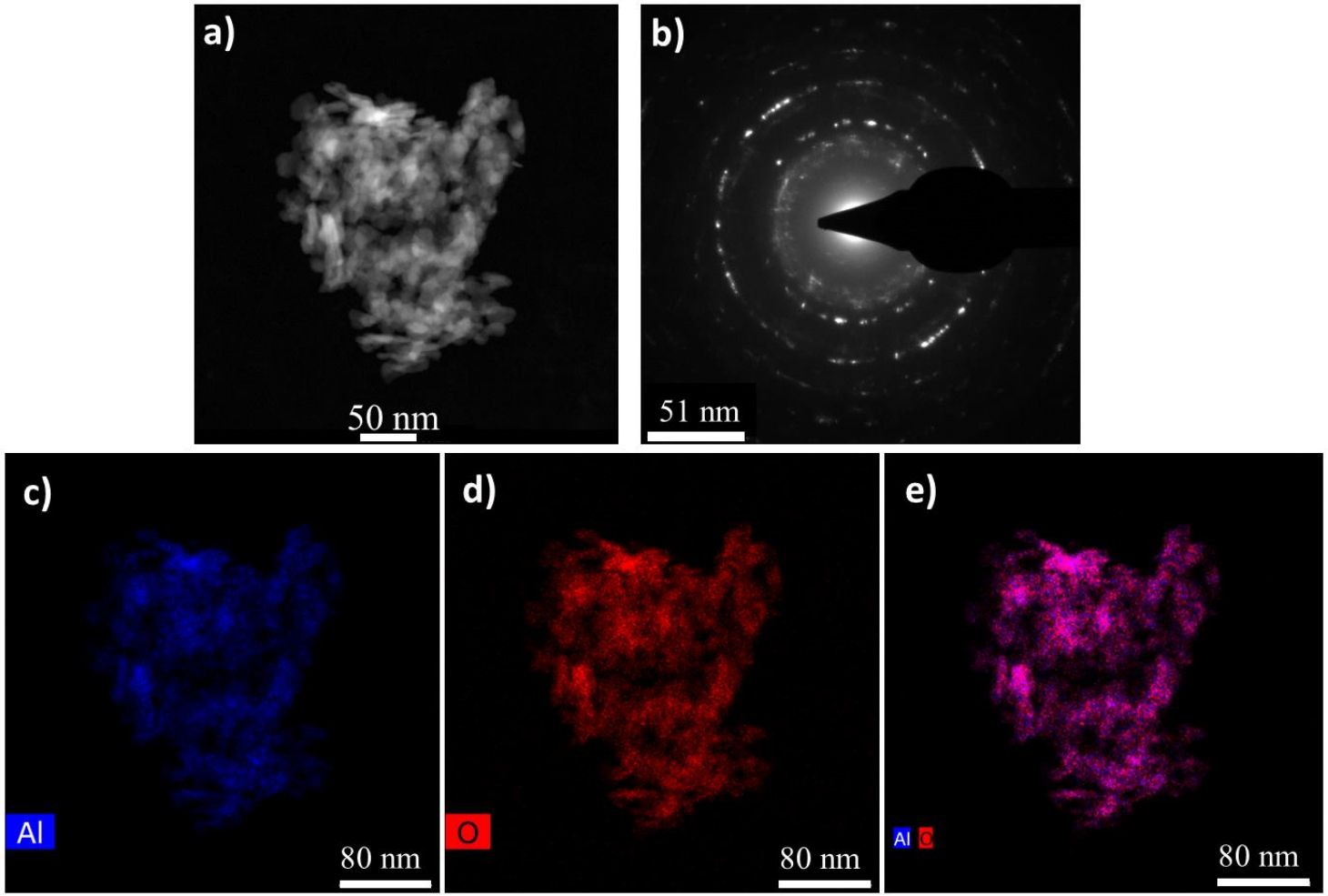

Figure S15. TEM and STEM analysis of the γ–Al_2O_3 nanoparticles (NPs). (a) HAADF-STEM micrograph of an aggregate of γ–Al_2O_3 NPs, (b) selected-area electron diffraction pattern recorded in TEM mode for the aggregate of NPs in (a) confirming the γ–Al_2O_3 cubic microstructure [7], and (c-e) element maps based on EDXS analysis in STEM mode for the aggregate of NPs shown in (a): (c) Al, (d) O and (e) Al-O.

Bibliography

[1] Y. Zhong, Q. Yang, K. Luo, X. Wu, X. Li, Y. Liu, W. Tang, G. Zeng, B. Peng, Fe(II)-Al(III) layered double hydroxides prepared by ultrasound-assisted co-precipitation method for the reduction of bromate, J. Hazard. Mater. 250–251 (2013) 345–353. doi:10.1016/j.jhazmat.2013.01.081.

[2] K. Asadpour-Zeynali, Y. Shabangoli, K. Nejati, Electrochemical synthesis of Fe/Al-layered double hydroxide on a glassy carbon electrode: Application for electrocatalytic reduction of isoniazid, J. Iran. Chem. Soc. 13 (2016) 29–36. doi:10.1007/s13738-015-0708-7.

[3] T. Peretyazhko, J.M. Zachara, S.M. Heald, R.K. Kukkadapu, C. Liu, A.E. Plymale, C.T. Resch, Reduction of Tc (VII) by Fe (II) Sorbed on Al (hydr)oxides, Environ. Sci. Technol. 42 (2008) 5499–5506.

[4] R.J. Lemire, U. Berner, C. Musikas, D.A. Palmer, P. Taylor, O. Tochiyama, Chemical Thermodynamics of Iron. Part 1, OECD Nucle, OECD, Paris, France, 2013.

[5] P.L. Brown, C. Ekberg, Hydrolysis of Metal Ions Vol 2, Wiley-VCH, Weinheim (Germany), 2016.

[6] R. Guillaumont, T. Fanghänel, V. Neck, J. Fuger, D.A. Palmer, I. Grenthe, M.H. Rand, Update on the chemical thermodynamics of Uranium, Neptunium, Plutonium, Americium and Technetium, OECD, Issy-les-Moulineaux (France)4, 2003.

[7] L. Smrcok, V. Langer, J. Krestan, gamma-alumina: a single-crystal X-ray diffraction study, Acta Crystallogr. Sect. A. C62 (2006) i83–i84.